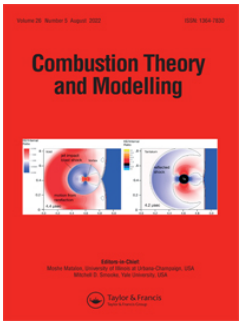

Combustion Theory and Modelling

ISSN: (Print) (Online) Journal homepage: https://www.tandfonline.com/loi/tctm20

Inward swirling flamelet model

William A. Sirignano

To cite this article: William A. Sirignano (2022): Inward swirling flamelet model, Combustion Theory and Modelling, DOI: 10.1080/13647830.2022.2103452

To link to this article: https://doi.org/10.1080/13647830.2022.2103452

Combustion Theory and Modelling, 2022
https://doi.org/10.1080/13647830.2022.2103452

Inward swirling flamelet model

William A. Sirignano*

Department of Mechanical and Aerospace Engineering, University of California, Irvine, CA, USA

(*Received 29 March 2022; accepted 12 July 2022*)

A new rotational flamelet model with inward swirling flow through a stretched vortex tube is developed for sub-grid modelling to be coupled with the resolved flow for turbulent combustion. The model has critical new features compared to existing models. (i) Non-premixed flames, premixed flames, or multi-branched flame structures are determined rather than prescribed. (ii) The effects of vorticity and the related centrifugal acceleration are determined. (iii) The strain rates and vorticity applied at the sub-grid level can be directly determined from the resolved-scale strain rates and vorticity without a contrived progress variable. (iv) The flamelet model is three-dimensional. (v) The effect of variable density is addressed. (vi) The inward swirl is created by vorticity combined with two compressive normal strain components; this feature distinguishes the model from counterflow flamelet models. Solutions to the multicomponent Navier–Stokes equations governing the flamelet model are obtained. By coordinate transformation, a similar solution is found for the model, through a system of ordinary differential equations. Vorticity creates a centrifugal force on the sub-grid counterflow that modifies the molecular transport rates, burning rates, and flammability limits. Sample computations of the inward swirling rotational flamelet model without coupling to the resolved flow are presented to demonstrate the importance of the new features. Premixed, nonpremixed, and multi-branched flame structures are examined. Parameter surveys are made with rate of normal strain, vorticity, Damköhler number, and Prandtl number. The centrifugal effect has interesting consequences when combined with the variable-density field. Flow direction can reverse; burning rates can be modified; flammability limits can be extended.

Keywords: flamelet; turbulent combustion; stretched vortex tube; similar solution; multi-branched flames

1. Introduction

The practical and major method for energy conversion for mechanical power and heating involves combustion in high mass-flux chambers. The high mass-flow rate leads to turbulent flow, whereby many length and time scales appear in the physics making serious challenges for both computational and experimental analyses. For computations where the smallest scales typically cannot be resolved, the method of large-eddy simulations (LES) is employed wherein the smaller scales are filtered via integration over a window size commensurate with the computational mesh size. This method allows affordable computations. However, the essential, rate-controlling, physical and chemical processes, occurring on shorter scales than the filter size, must be modelled. In the computations, those sub-grid models must be properly coupled to the resolved LES flow field.

*Corresponding author. Email: sirignan@uci.edu

Currently, flamelet models are often used for LES or Reynolds-averaged Navier–Stokes (RANS) methods with some advantages. The flamelet equations are usually a system of ordinary differential equations (ODEs) to be solved offline with solutions available in tabular form or through neural networks (NN). The most popular flamelet models can handle multi-species, multi-step oxidation kinetics without requiring small time steps during the solution of the resolved-scale fluid dynamics. Thus, savings of computational resources can be major compared to direct numerical simulation. Here, we will retain these very attractive features while removing some less desirable features. Already, some progress has been made in extending the fundamental flamelet theory beyond its long-term limitation of a single-flame structure, two-dimensional (or axisymmetric) configuration, and use of the uniform-density assumption. Still, those advances must be applied to LES or RANS. In addition, the flamelet theory must consider shear strain and vorticity at the small scale of the flamelet; these are the vital forgotten physics in current flamelet modelling. Furthermore, the strain rates in the flamelet model are far from properly connected to the strain rates at the resolved scale.

The goals in this paper are to improve the flamelet model by including several important physical effects that are commonly neglected in present models and to identify other issues, related to the coupling between the sub-grid-scale physics and the resolved-scale (or time-averaged) physics, that require further study.

1.1. *Existing flamelet theory*

The laminar mixing and combustion that occur within the small turbulent eddies determines the performance for many power and propulsion applications. These laminar flamelet sub-domains experience significant shear, tensile, and compressive strains. Some important works exist here but typically for either counterflows with only normal strain or simple vortex structures in planar or axisymmetric geometry and often with a constant-density approximation. See Linan [1], Williams [2], Marble [3], Karagozian and Marble [4]), Cetegen and Sirignano [5,6], Peters [7], and Pierce and Moin [8]. Only Karagozian and Marble, in one of their two problems, address a stretched vortex with an inward swirling flow which is the topic of this current paper. An interesting review of the early flamelet theory is given by Williams [9]. Williams [2] first established the concept of laminar flamelets in the turbulent diffusion flame structure. Flamelet studies have focussed on either premixed or nonpremixed flames; a unifying approach to premixed, nonpremixed, and multi-branched flames has not been developed until the recent counterflow-based rotational flamelet study by Sirignano [10]. Here, we attempt a unification for the vortex-tube-based flamelet.

Most flamelet studies do not directly consider vorticity interaction with the flamelet; examples are [1,7–9]. Williams [2] first recognised the advantage of separating rotation (due to vorticity) and stretching by transformation to a rotating, non-Newtonian reference frame. However, the momentum consequences in the new reference frame were not examined. Some other works that have examined vortex-flame interaction have not included the effects of stretching and rotation [3,5,6,11]. In one of two problems treated in their paper, Karagozian and Marble [4] examined a three-dimensional flow with radial inward velocity, axial jetting, and a vortex centred on the axis. The flame sheet wrapped around the axis due to the vorticity; an incompressible-flow velocity field was used with an ad hoc adjustment for the variable density effect. However, that adjustment could not account for the density gradients and associated centrifugal effects to be discussed here.

Our interest on high-mass-flux turbulent combustors leads to a focus on situations with a wide range of length and time scales where shearing, reactant mixing, and exothermic reaction occur together. Thus, mention here of many interesting areas of turbulent-combustion literature is avoided, e.g. corrugated (i.e. wrinkled) premixed, laminar flames.

The two-dimensional planar or axisymmetric counterflow configuration is commonly the foundation for a flamelet model. Coordinate-system change based on the principal strain-rate directions can provide the counterflow configuration in a general flow. Furthermore, the quasi-steady counterflow can be analysed by ordinary differential equations because the dependence on the transverse coordinate is either constant or linear, depending on the variable. Pierce and Moin [8] modified the nonpremixed-flamelet counterflow configuration by fixing domain size and forcing flux to zero at the boundaries. Flamelet theory as a closure model for turbulent combustion typically tracks two resolved-scale variables: a normalised conserved scalar and the strain rate. Generally, the strain rate is given indirectly through a progress variable. The progress variable is not a fundamental parameter and must be defined in some arbitrary fashion. Mixture fraction is traditionally used for the conserved scalar. The flamelet model for LES developed by Pierce and Moin [8] was a substantial advancement through the introduction of the flamelet progress variable (FPV). Their approach has also been used widely, e.g. [12–15]. Some [12,16,17] introduced the use of neural networks in place of the look-up table. Mueller [18] presented the flamelet model in a somewhat different mathematical framework but without the addition of a new physical description. Nevertheless, there are concerns about incompleteness and contradiction in the above models. (i) The models are designed specifically for nonpremixed flames or premixed flames. The flame structure should be determined rather than prescribed. Multi-branched flames should be allowed. (ii) The effects of vorticity are commonly neglected with a very few exceptions identified above. Yet, the models are applied to turbulent flows where the strain rates and vorticity magnitudes are known to be larger at the small scales than at the large scales. (iii) The above flamelet models are two-dimensional or axisymmetric although key three-dimensional behaviour can be shown to exist. (iv) The effect of variable density is not thoroughly addressed. (v) Clear connections are not given between the strain rates and vorticity at the flamelet level and those variables at the resolved scale of the combustor. Sirignano [10] has addressed the incompleteness and contradiction for counterflow flamelets with the presentation of a rotational flamelet closure model. Here, we attempt to follow with consideration of flamelets in vortex tubes.

1.2. *Stretched vortex with inward swirl*

In one part of their paper, Karagozian and Marble [4] treated a flame within a stretched vortex tube with an inward swirling flow. Their incompressible velocity field was defined by Burgers [19] and Rott [20] and is commonly known as Burgers vortex. In particular, with u_r, u_z, and u_θ as the velocity components in cylindrical coordinates and parameter a and kinematic viscosity ν taken as constants, we have

$$u_r = ar; \quad u_z = 2az$$
$$u_\theta = \frac{\Gamma}{4\pi r}\left[1 - \exp\left(-\frac{ar^2}{2\nu}\right)\right] \tag{1}$$

where Γ is the circulation taken through the far field surrounding the vortex tube. Note that $u_\theta \to \Gamma/(2\pi r)$ as $r \to \infty$, yielding potential flow for the far field. This description gives

an exact steady-state solution to the incompressible Navier–stokes equations. Although the tube is being stretched in the z direction, diffusion of momentum and vorticity in the r direction allows a balance with radial advection that results in a steady solution.

Karagozian and Marble [4] made an ad hoc adjustment to correct for expansion by variable density; however, by not accounting for spatial variation of density, the effect of centrifugal acceleration was not considered. They also focussed on diffusion flames. Here, a stretched vortex will be considered but with full account of variable density and allowance for a premixed flame, multibranched flame, or diffusion flame as determined by the boundary conditions. We will not use the incompressible Burgers vortex velocity field; however, it does provide useful guidance. In particular, note that for small r values, the Burgers vortex gives wheel motion for the fluid, i.e. $u_\theta \approx (\Gamma a r)/(4\pi\nu)$.

1.3. *Relative orientations of principal strain axes, vorticity, and scalar gradients*

Both normal strain rate and shear strain rate are imposed on the flamelet and are important. Shear strain can, in general, be decomposed into a normal strain and a rotation (whose rate is half of the vorticity magnitude). The magnitudes of strain rate and vorticity increase as the eddy size decreases in the turbulence energy cascade. The strain and rotation become especially important on the smallest turbulence scales where mixing and chemical reaction occur. The dissipation rate of turbulence kinetic energy determines the smallest (i.e. Kolmogorov) scale size. The final molecular mixing and chemical reaction occur on this smaller scale, where there will be an axis (or direction) of principal compressive normal strain and an orthogonal axis for principal tensile strain, the third orthogonal axis could be either tensile or compressive. These axes rotate due to vorticity. Thereby, the direction of the scalar gradient rotates. A useful flamelet model must have a statistically accurate representation of the relative orientations on this smallest scale of the vorticity vector, scalar gradients, and the directions of the three principal axes for strain rate. Several studies are helpful in understanding this important alignment issue [21–25].

Generally (and always for incompressible flow), at least one principal strain rate γ locally will be compressive (corresponding to inflow in a counterflow configuration), another principal strain rate α will be tensile (also named extensional and corresponding to outflow), and the third can be either extensional or compressive and will have an intermediate strain rate β of lower magnitude than the other like strain rate. Specifically, $\alpha > \beta > \gamma, \alpha > 0, \gamma < 0$, and, for incompressible flow, $\alpha + \beta + \gamma = 0$. If the intermediate strain rate $\beta < 0$, there is inflow from two directions with outflow in one direction; a contracting jet flow occurs locally. Conversely, with $\beta > 0$, there is outflow in two directions and inflow in one direction; a counterflow or, in other words, the head-on collision of two opposed jets occurs.

Direct numerical simulations (DNS) for incompressible flows have provided some useful guidance. Both Ashurst et al. [21] and Nomura and Elghobashi [22] compared a case of homogeneous sheared turbulence with a case of isotropic turbulence. The vorticity alignment with the intermediate strain direction is most probable in both cases but especially in the case with shear. Furthermore, the intermediate strain rate is most likely to be extensive (positive) implying a counterflow configuration.

Nomura and Elghobashi [23] show for reacting flow that, in regions of exothermic reaction and variable density, alignment of the vorticity with the most tensile strain direction can occur. Still, as the strain rates increase, the intermediate direction again becomes more

favoured for alignment with vorticity; that direction is also preferred in regions where mixing occurs without substantial divergence of the velocity due to chemical reaction.

A material interface most probably aligns to be normal to the direction of the compressive normal strain. That is, the scalar gradient and the direction of compressive strain are aligned [21–25]. There is agreement that the most common intermittent vortex structures in regions of high strain rate are sheets or ribbons rather than tubes. Nevertheless, the agreement is that vortex tubes can exist in a combustor and can be relevant.

Based on those understandings concerning vector orientations, flamelet theory was extended [26] in a second significant aspect beyond the inclusion of both premixed and non-premixed flame structures; namely, a model was created of a three-dimensional field with both shear and normal strains. The three-dimensional problem is reduced to a two-dimensional form and then, for the counterflow or mixing-layer flow, to a one-dimensional similar form. The system of ordinary differential equations (ODEs) is presented for the thermo-chemical variables and the velocity components. Conserved scalars are determined and can become the independent variable if they behave in a monotonic fashion. These new findings are very helpful in improving the foundations for flamelet theory and its use in sub-grid modelling for turbulent combustion.

With attention to the needed improvements, a new rotational flamelet model was recently developed based on a counterflow with rotation [10]. The model (i) determines rather than prescribes the existence of non-premixed flames, premixed flames, or multi-branched flame structures; (ii) determines directly the effect of shear strain and vorticity on the flames; (iii) applies directly the resolved-scale strain rates and vorticity to the sub-grid level without the use of a contrived progress variable; (iv) employs a three-dimensional flamelet model; (v) considers the effect of variable density. The goal with the new inward-swirl flamelet model presented here is to extend these five above-mentioned attributes of the rotational flamelet concept to a new vortex-tube configuration with inward spiralling flow rather than the traditional counterflow. Elements of the counterflow character will remain because fluid of differing compositions will be strained to move towards each other enhancing transport and reaction. The earlier analysis [10] as well as this new analysis use one-step kinetics to avoid complications in these initial studies; however, a clear template will exist for the future employment of multi-step kinetics.

Section 2 presents the analysis supporting a new sub-grid flame model that better addresses effects of rotation, variable density, three-dimensional character, and multi-branched flame structure for the stretched vortex tube Computational results are discussed in Section 2. Results and the related discussion are presented in Section 3. Concluding comments are made in Section 4.

2. Flamelet analysis

The problem is stated here in a quasi-steady, three-dimensional form where variable density is allowed. These assumed orientations are consistent with the statistical findings of [23]. The direction of major compressive principal strain aligns with the scalar gradient and is orthogonal to the vorticity vector direction; an extensional principal strain direction is aligned with the vorticity. The stretched vortex character is created by imposing compressive normal strain in both coordinate directions that are orthogonal to the vorticity vector. Thus, we have a stretched vortex tube that qualitatively relates to the incompressible-flow, uniform-density configurations of [19,20], and [4].

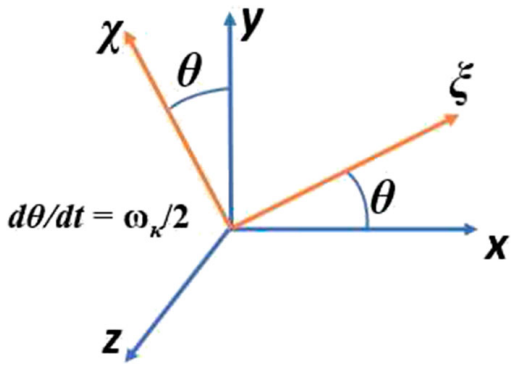

Figure 1. Transformation to ξ, χ, z' rotating coordinate system from x', y', z' Newtonian system. θ increases in the counterclockwise direction.

The analysis here will have many identical features to those presented in [10]. The essential differences between the current analysis and the prior analysis for the rotational flamelet is that here we have compressive normal strain (i.e. inflow) imposed in two directions with extensional normal strain (i.e. outflow) in one direction while, there earlier, compressive normal strain (i.e. inflow) occurred in only one direction with outflow in two directions. The inward spiral of the flow can only occur with two compressive normal strain directions. Consequently, the governing equations will look identical; however, the difference in the signs of imposed normal strain rates has major physical consequence.

Major differences of this new analysis with the analyses of [4,19,20] are present. Those analyses were axisymmetric with uniform density. Here, both three-dimensionality and density gradients are essential to capture the centrifugal effect that will be seen to modify burning rates. Three-dimensional behaviour will occur when a direction for scalar gradients is identified. It also may be enhanced if the two inward flowing streams have strain rates of differing magnitudes.

2.1. *Coordinate transformation*

In Figure 1, the Newtonian frame is transformed to a rotating, non-Newtonian frame where the curl of the velocity is zero. The vorticity aligns with the z' direction. ω_κ is the vorticity magnitude on this sub-grid (Kolmogorov) scale. x, y, z are transformed to ξ, χ, z wherein the material rotation is removed from the ξ, χ plane by having it rotate at angular velocity $\mathrm{d}\theta/\mathrm{d}t = \omega_\kappa/2$ relative to x, y. Here, θ is the angle between the x and ξ axes and simultaneously the angle between the y and χ axes. The sub-grid domain is sufficiently small to consider a uniform value of ω across it, consistent with the truncated Taylor series expansion used elsewhere in the flamelet analysis. The scalar gradients align with the major principal axis for compressive strain. In many of our calculations, the two compressive normal strains will have equal magnitude; so, the choice of the normal strain direction which aligns with the scalar gradient is arbitrary. The scalar gradient is always aligned with the χ direction in the analysis here.

Thereby,

$$\xi = x\cos\theta + y\sin\theta; \quad \chi = y\cos\theta - x\sin\theta$$

$$\frac{\partial\xi}{\partial x} = \cos\theta; \quad \frac{\partial\xi}{\partial y} = \sin\theta; \quad \frac{\partial\chi}{\partial x} = -\sin\theta; \quad \frac{\partial\chi}{\partial y} = \cos\theta$$

$$u_\xi = u\cos\theta + v\sin\theta + \chi\frac{\omega_\kappa}{2}; \quad u_\chi = v\cos\theta - u\sin\theta - \xi\frac{\omega_\kappa}{2}$$
$$\frac{\partial u}{\partial x} = \frac{\partial u}{\partial \xi}\cos\theta - \frac{\partial u}{\partial \chi}\sin\theta; \quad \frac{\partial u}{\partial y} = \frac{\partial u}{\partial \xi}\sin\theta + \frac{\partial u}{\partial \chi}\cos\theta$$
$$\frac{\partial v}{\partial x} = \frac{\partial v}{\partial \xi}\cos\theta - \frac{\partial v}{\partial \chi}\sin\theta; \quad \frac{\partial v}{\partial y} = \frac{\partial v}{\partial \xi}\sin\theta + \frac{\partial v}{\partial \chi}\cos\theta \tag{2}$$

Since

$$\frac{\partial v}{\partial x} - \frac{\partial u}{\partial y} = \omega_\kappa \tag{3}$$

it follows that

$$\frac{\partial u_\chi}{\partial \xi} - \frac{\partial u_\xi}{\partial \chi} = 0 \tag{4}$$

Thus, the rotating frame of reference does not have vorticity appearing explicitly. However, the frame is not Newtonian and a reversed (centrifugal) force is imposed. The expansions due to energy release produce new vorticity but it will integrate to zero globally; the flow will be antisymmetric and have zero circulation in the new reference frame.

In the new reference frame, the normal rates of strain, imposed in the far field, in the ξ, χ, and z directions are S_1, $-(S_1 + S_2)$, and S_2, respectively. Sirignano [10], for the rotational flamelet with counterflow, considered both S_1 and S_2 to be positive. Here, with the inward swirl flamelet, $S_1 < 0,\ S_2 > 0$, and $S_1 + S_2 > 0$. In the next sub-section, these strain rates will be non-dimensionalized.

2.2. *Governing equations*

Quasi-steady behaviour is considered. The governing equations for steady 3D flow in the non-Newtonian frame can be written with $u_i = u_\xi, u_\chi, w$; $x_i = \xi, \chi, z$. The centrifugal acceleration $a_i = \xi\omega_\kappa^2/4,\ \chi\omega_\kappa^2/4,\ 0$. The quantities $p, \rho, h, h_m, Y_m, \dot{\omega}, \mu, \lambda, D$, and c_p are pressure, density, specific enthalpy, heat of formation of species m, mass fraction of species m, chemical reaction rate of species m, dynamic viscosity, thermal conductivity, mass diffusivity, and specific heat, respectively. Furthermore, the Newtonian viscous stress tensor with the Stokes hypothesis is considered. The boundary-layer approximation is not needed and the Navier–Stokes equations for a multicomponent field will be solved. The system is described as

$$\frac{\partial(\rho u_j)}{\partial x_j} = 0 \tag{5}$$
$$\rho u_j\frac{\partial u_i}{\partial x_j} + \frac{\partial p}{\partial x_i} = \frac{\partial}{\partial x_j}\left(\mu\left[\frac{\partial u_i}{\partial x_j} + \frac{\partial u_j}{\partial x_i} - \frac{2}{3}\delta_{ij}\frac{\partial u_k}{\partial x_k}\right]\right) + \rho a_i \tag{6}$$
$$\rho u_j\frac{\partial h}{\partial x_j} = \frac{\partial}{\partial x_j}\left(\frac{\lambda}{c_p}\frac{\partial h}{\partial x_j}\right) + \frac{\partial}{\partial x_j}\left(\rho D(1-Le)\Sigma_{m=1}^{N} h_m\frac{\partial Y_m}{\partial x_j}\right) - \rho\Sigma_{m=1}^{N} h_{f,m}\dot{\omega}_m \tag{7}$$
$$\rho u_j\frac{\partial Y_m}{\partial x_j} = \frac{\partial}{\partial x_j}\left(\rho D\frac{\partial Y_m}{\partial x_j}\right) + \rho\dot{\omega}_m; \quad m = 1, 2, \ldots, N \tag{8}$$

The viscous dissipation, the energy source term $\rho u_j a_j = \rho(\omega_\kappa/2)^2(\xi u_\xi + \chi u_\chi)$ in the new reference frame, and other terms of the order of the kinetic energy per mass have been neglected.

Here, we define the non-dimensional Prandtl, Schmidt, and Lewis numbers: $Pr \equiv c_p\mu/\lambda$; $Sc \equiv \mu/(\rho D)$; and $Le \equiv Sc/Pr$. These numbers will be assumed to be constants. Furthermore, $Pr = Sc$ (i.e. $Le = 1$).

The non-dimensional forms of the above equations remain identical to the above forms if we choose certain reference values for normalisation. In the remainder of this article, the non-dimensional forms of the above equations will be considered. The superscript * is used here to designate a dimensional property. The variables $u_i^*, t^*, x_i^*, \rho^*, h^*, p^*$, and $\dot{\omega}_m^*$, and properties $\mu^*, \lambda^*/c_p^*$, and D^* are normalised respectively by $[(S_1^* + S_2^*)\mu_\infty^*/\rho_\infty^*]^{1/2}, (S_1^* + S_2^*)^{-1}, [\mu_\infty^*/(\rho_\infty^*(S_1^* + S_2^*))]^{1/2}, \rho_\infty^*, (S_1^* + S_2^*)\mu_\infty^*/\rho_\infty^*, (S_1^* + S_2^*)\mu_\infty^*, (S_1^* + S_2^*), \mu_\infty^*, \mu_\infty^*$, and $\mu_\infty^*/\rho_\infty^*$. The dimensional strain rates S_1^* and S_2^* and vorticity ω_κ^* are normalised by $S_1^* + S_2^*$. The reference values for strain rates and far-stream variables and properties used for normalisation will be constants. The reference length $[\mu_\infty^*/(\rho_\infty^*(S_1^* + S_2^*))]^{1/2}$ is the estimate for the magnitude of the viscous-layer thickness. In the following flamelet analysis, the vorticity ω_κ and the velocity derivatives $\partial u_i/\partial x_j$ are non-dimensional quantities; their dimensional values can be obtained through multiplication by $S_1^* + S_2^*$. Now, $S_1 + S_2 = 1$.

In the rotating reference frame, two different gaseous mixtures exist in the far field, one for large positive values of χ and another for large negative values of χ. They both advect and diffuse towards each other. For the study of a diffusion (nonpremixed) flame, one mixture is fuel and the other is an oxidiser. With a premixed flame, one far field has a combustible mixture of fuel and oxidiser while the other has a hot inert gas (e.g. combustion products). In another case where multiple flame branches may occur, both streams can be combustible; one can be fuel rich while the other is fuel lean.

2.3. *Similar form for the equations*

The stagnation point is taken as the origin $\xi = \chi = z = 0$. Along the line $\xi = z = 0$ normal to the interface, we can expect the first derivatives of u_χ, ρ, h, T, and Y_m with respect to either ξ or z to be zero-valued. The velocity components u_ξ and w will be odd functions of ξ and z, respectively, going through zero and changing sign at that line. v also changes sign, going through zero at the origin; however, generally the reaction zone will be offset and an odd function does not result for v. Upon neglect of terms of $O(\xi^2)$ and $O(z^2)$, the variables u_χ, ρ, h, T, and Y_m can be considered to be functions only of t and χ. The density-weighted Illingworth transformation [27] of χ replaces χ with $\eta \equiv \int_0^y \rho(\chi')\,\mathrm{d}\chi'$. Neglect of terms of the same order of magnitude implies that $u_\xi = S_1\xi(\mathrm{d}f_1/\mathrm{d}\eta)$ and $w = S_2 z(\mathrm{d}f_2/\mathrm{d}\eta)$. Note u_ξ is independent of z and w is independent of ξ). At the edge of the viscous layer at large positive η, $\mathrm{d}f_1/\mathrm{d}\eta \to 1, \mathrm{d}f_2/\mathrm{d}\eta \to 1, f_1 \to \eta$, and $f_2 \to \eta$. Ordinary differential equations are created here through the variable η and the convenient notation is used so that $()' \equiv \mathrm{d}()/\mathrm{d}\eta$.

In the non-dimensional form given by Equations (5) through (8), the dimensional strain rates S_1^* and S_2^* are each normalised by the dimensional sum $S* = S_1^* + S_2^*$. If the far field has uniform density, $S*$ is the magnitude of the major compressive normal strain. Thus, the non-dimensional relation is $S_2 = 1 - S_1$ and only one independent non-dimensional strain-rate parameter is needed. Two strain rates are presented above and in the following analysis with the understanding that one depends on the other such that $S_1 + S_2 = 1$. $S_1 + S_2$ will be explicitly stated in our analysis without substitution of the unity value in order to emphasise

the summation which is consequential in the dimensional formulation. This choice clarifies whether a particular term when converted to a dimensional form depends on S_1^*, S_2^*, or the sum of the two strain rates.

The analysis follows closely the method of [10]. Here, that method is presented in a summary fashion since details are readily available. For the steady state, the continuity Equation (5) is integrated to give

$$\rho u_\chi = -S_1 f_1(\eta) - S_2 f_2(\eta) \tag{9}$$

and then

$$u'_\chi = \frac{S_1 f_1(\eta) + S_2 f_2(\eta)}{\rho^2}\rho' - \frac{S_1 f_1'(\eta) + S_2 f_2'(\eta)}{\rho} \tag{10}$$

Thus, the incoming inviscid flow outside the boundary layer is described by $u_\chi = -(S_1 + S_2)\eta$ for positive η and $u_\chi = -(S_1 + S_2)\eta/\rho_{-\infty}$ for negative η.

At $\eta = \infty$, $f_1' = f_2' = 1$ and $f_1'' = f_2'' = f_1''' = f_2''' = 0$ which allows the two constants to be determined. A perfect gas with $\rho\mu = 1$ is assumed. The perfect-gas law and the assumption of constant specific heat c_p will give the relation that $1/\rho = h$. Following the earlier analysis [10], the pressure gradient in the η direction can be shown to be a function of η only. Thereby, $\partial^2 p/\partial\eta\partial z = 0$ and $\partial^2 p/\partial\eta\partial\chi = 0$. This implies that $\partial p/\partial z$ and $\partial p/\partial\chi$ are independent of η. Consequently, certain constants appear in the z-momentum equation and the χ-momentum equation. These two constants are determined by the boundary condition on the momentum equations. Specifically, we obtain

$$\begin{aligned} f_1''' + f f_1'' + S_1[h - (f_1')^2] + \frac{\omega_\kappa^2}{4S_1}(1-h) = 0 \\ f_2''' + f f_2'' + S_2[h - (f_2')^2] = 0 \end{aligned} \tag{11}$$

The boundary conditions use the assumption that two velocity components asymptote to the constant values $u_\xi(\infty), u_\xi(-\infty), w(\infty)$, and $w(-\infty)$ at large magnitudes of η. The stream function bounding the two incoming streams is arbitrarily given a zero value and placed at $\eta = 0$.

$$\begin{aligned} &f_1'(\infty) = 1; \quad f_1'(-\infty) = \sqrt{h_{-\infty} + \left(\frac{\omega_\kappa}{2S_1}\right)^2 (1 - h_{-\infty})}; \quad f_1(0) = 0; \\ &f_2'(\infty) = 1; \quad f_2'(-\infty) = \sqrt{h_{-\infty}}; \quad f_2(0) = 0 \end{aligned} \tag{12}$$

When density varies through the flow because of heating or variation of composition, u_ξ and w vary with χ, thereby creating a shear stress and vorticity albeit that the frame transformation removed vorticity and shear from the incoming flow.

The dependence of u_χ on $f \equiv S_1 f_1 + S_2 f_2$ is shown by Equation (9). Thus, the function f will be important in determining both the field for u_χ and the scalar fields.

Consequently, f as well as f_1 and f_2 depend on both S_1 and S_2, not merely on $S_1 + S_2$. That is, the particular distribution of the normal strain rate between the two transverse directions matters. f and f_1 also depend directly on ω_κ (unless $S_1 = 0$). f_2 depends on ω_κ indirectly through its coupling with f_1.

Here, an exact solution of the variable-density Navier–Stokes equation is obtained subject to determination of h through solutions of the energy and species equations as

discussed below. Thus, the solution here is the natural solution, subject to neglect of terms of $O(\xi^2)$ and $O(z^2)$.

The similar form of the scalar equations becomes

$$\begin{aligned} Y_m'' + PrfY_m' &= -Pr\dot{\omega}_m; \quad m = 1, 2, \ldots, N \\ h'' + Prfh' + (Pr - Sc)\Sigma_{m=1}^{N} h_m Y_m'' &= Pr\Sigma_{m=1}^{N} h_{f,m}\dot{\omega}_m \end{aligned} \tag{13}$$

The boundary conditions are

$$\begin{aligned} h(\infty) = 1; \quad h(-\infty) &= \frac{1}{\rho_{-\infty}}; \\ Y_m(\infty) = Y_{m,\infty}; \quad Y_m(-\infty) &= Y_{m,-\infty}; \end{aligned} \tag{14}$$

Equation (13) indicate a dependence of the heat and mass transport on $f \equiv S_1 f_1 + S_2 f_2$. Manipulation of the first two equations of (13) leads to an ODE for f with $S_1 S_2$ and $S_1 S_2 f_1' f_2'$ as parameters, clearly indicating that generally f will have a dependence on $S_1 S_2$. Thus, the behaviour for the counterflow can vary from the planar value of $S_1 = 1, S_2 = 0$ (or vice versa) or from the case $S_1 = S_2 = 1/2$. This clearly shows that distinctions must be made amongst the various possibilities for three-dimensional strain fields as $S_1 S_2$ varies between large negative numbers and 1/4. An exception is the incompressible case with constant properties where the $S_1 S_2$ terms cancel in the equation for f.

The vorticity ω_κ impacts directly f_1 and f; thereby, it is affecting the velocity field. Then, through the advection of the scalar properties, there is impact on mass fractions and enthalpy. If the vorticity $\omega_\kappa = 0$, a simple inspection of the governing ODEs leads to the conclusion that the values for $f_1, f_1', f_2, f_2', u/x$, and w/z can be interchanged with the values for $f_2, f_2', f_1, f_1', w/z$, and u/x, respectively, when S_1 and S_2 are replaced by $1 - S_1$ and $1 - S_2$, respectively.

The analysis is formulated in identical fashion to the approach of [10]. However, there, with two directions for extensional strain rate in the rotating frame of reference, both S_1 and S_2 are positive numbers. However, in the computations here, we consider the vortex tube with inward swirl so that, in the far field, there are two directions of compressive strain and only one direction of extensional strain. That extensional strain is aligned with the vorticity vector. Thus, here, $S_1 \leq 0$ and $S_2 \geq 1$. The basic case takes the two compressive strain rates to be equal; thereby, $S_1 = -1.0$ and $S_2 = 2.0$.

Consider the production or consumption rate of a particular species over the counterflow volume. We can either integrate over a volume using the original form in Equation (8) or, more conveniently, using Equation (13) to get exactly the same result. Consider the volume $-a < \xi < a, -b < y < b, -c < z < c$. The choices of lengths a and c do not matter on a per-unit-volume basis since mass fraction Y_m and reaction rate $\dot{\omega}_m$ do not vary with x or z. c is chosen to be of the order of the Kolmogorov scale. Volume $V = 8abc$ and $\widetilde{\rho\dot{\omega}_m}$ is the average mass production rate over the volume. From integration of Equation (13) after multiplication by density ρ and division by PrV,

$$\int_{-a}^{a}\int_{-b}^{b}\int_{-c}^{c} \frac{\rho}{PrV}[Y_m'' + PrfY_m' + Pr\dot{\omega}_m]\,\mathrm{d}x\,\mathrm{d}y\,\mathrm{d}z = 0; \quad m = 1, 2, \ldots, N$$

$$\widetilde{\rho\dot{\omega}_m} \equiv \frac{1}{V}\int_V \rho\dot{\omega}_m\,\mathrm{d}V = -\frac{1}{2b}\int_{\eta(-b)}^{\eta(b)} fY_m'\mathrm{d}\eta; \quad m = 1, 2, \ldots, N$$

$$\int_{-a}^{a}\int_{-b}^{b}\int_{-c}^{c}\frac{\rho}{PrV}[h''+Prfh'-Pr\Sigma_{m=1}^{N}h_{f,m}\dot{\omega}_m]\,\mathrm{d}x\,\mathrm{d}y\,\mathrm{d}z=0$$

$$\Sigma_{m=1}^{N}h_{f,m}\widetilde{\rho\dot{\omega}_m}=\frac{1}{2b}\int_{\eta(-b)}^{\eta(b)}fh'\,\mathrm{d}\eta \tag{15}$$

Here, b is considered large enough so that $\widetilde{Y_m'}=0$ and $h'=0$ at those boundaries are good approximations. However, the value for $\widetilde{\rho\dot{\omega}_m}$ depends strongly on the chosen domain size $2b$, which has a value of $O(10)$ typically in our analysis.

Consider a species m that is flowing inward away from $\eta=\infty$ towards $\eta=0$. If it is being produced (consumed), the derivative Y_m' in Equation (15) will be negative (positive) for $\eta>0$ where velocity $v<0$ and $f>0$. The signs are opposite for a species flowing inward away from $\eta=-\infty$ and towards $\eta=0$. The equation provides two ways to evaluate the average production (consumption) rate for species m. The volume integral of the reaction rate has highly nonuniform integrand values over the space while the outflow integral over η has a smoother variation of the integrand.

2.4. *Chemical kinetics model*

The above analysis applies for both diffusion-flame and partially-premixed-flame configurations. Multi-branched flames can also be described. While the analysis allows for the use of detailed chemical kinetics, we focus here on propane-oxygen flows with one-step kinetics. Westbrook–Dryer [28] kinetics are used; they were developed for premixed flames but any error for nonpremixed flames is often viewed as tolerable here because diffusion generally is rate-controlling. Using asterisks to denote dimensional quantities,

$$\dot{\omega}_F^*=-A^*{\rho^*}^{0.75}Y_F^{0.1}Y_O^{1.65}\,\mathrm{e}^{-50.237/\tilde{h}} \tag{16}$$

where the ambient temperature is set at 300 K and density ρ^* is to be given in units of kilograms per cubic meter. $A^*=4.79\times10^8\,(\mathrm{kg/m^3})^{-0.75}/\mathrm{s}$. The dimensional strain rate $S_1^*+S_2^*$ (at the sub-grid scale) is used to normalise time and reaction rate. In non-dimensional terms,

$$\dot{\omega}_F=-\frac{A^*{\rho_\infty^*}^{0.75}}{S_1^*+S_2^*}\tilde{h}^{-0.75}Y_F^{0.1}Y_O^{1.65}\,\mathrm{e}^{-50.237/\tilde{h}}$$

$$\dot{\omega}_F=-\frac{Da}{\tilde{h}^{0.75}}Y_F^{0.1}Y_O^{1.65}\,\mathrm{e}^{-50.237/\tilde{h}} \tag{17}$$

The equation defines the Damköhler number Da. We define K so that $Da\equiv KDa_{ref}$ where

$$Da_{ref}\equiv\frac{\tilde{A}(10\,\mathrm{kg/m^3})^{0.75}}{(10^4/\mathrm{s})}=2.693\times10^5;\quad K\equiv\left[\frac{\rho_\infty^*}{10\,\mathrm{kg/m^3}}\right]^{0.75}\frac{10^4/\mathrm{s}}{S_1^*+S_2^*} \tag{18}$$

$10\,\mathrm{kg/m^3}$ and 10,000/s are conveniently chosen as reference values for density and strain rate, respectively.

The flow in the flame region will have a very low Mach number; thereby, for the purposes of the energetics and the thermodynamics, the pressure can be considered to be well approximated as uniform. Pressure gradients need to be considered only for the momentum equations. Thus, in addressing chemical kinetics, the pressure is taken as uniform

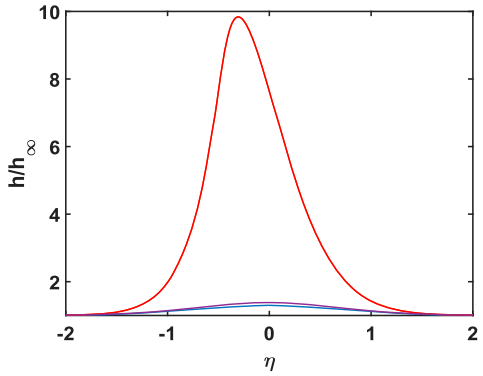

(a) enthalpy, h/h_∞

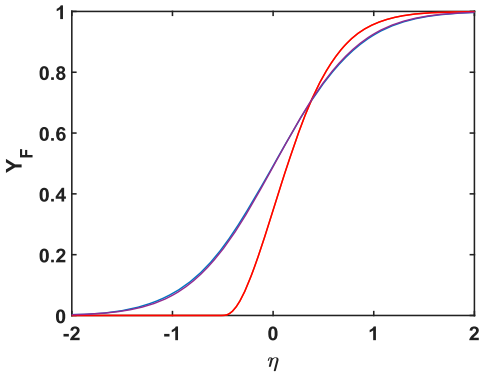

(b) fuel mass fraction, Y_F

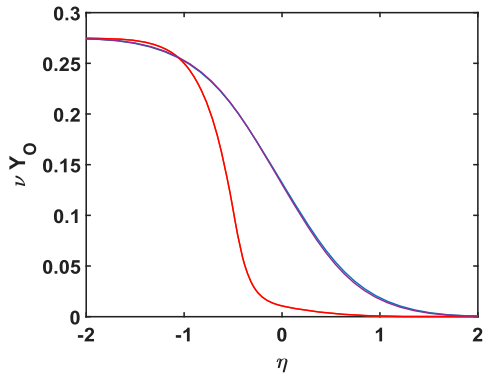

(c) mass ratio x oxygen mass fraction, νY_O

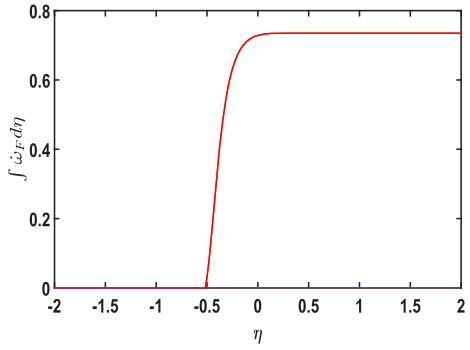

(d) integral of reaction rate, $\int \dot{\omega}_F d\eta$

Figure 2. Scalar properties for diffusion flame with varying vorticity. $S_1 = -1.00$; $S_2 = 2.00$; $K = 0.275$. $\omega_\kappa = 0$, blue, no flame; $\omega_\kappa = 0.5$, purple, no flame; $\omega_\kappa = 1.0$, red, flame. (a) enthalpy, h/h_∞; (b) fuel mass fraction, Y_F; (c) mass ratio x oxygen mass fraction, νY_O; (d) integral of reaction rate, $\int \dot{\omega}_F \mathrm{d}\eta$.

over the field. It is not necessary to set pressure (or its proxy, density) and the strain rate separately for a one-step reaction. For propane and oxygen, the mass stoichiometric ratio $\nu = 0.275$. The non-dimensional parameter K will increase (decrease) as the strain rate decreases (increases) and/ or the pressure increases (decreases). $K = 1$ is our reference case. The value of K will be varied as needed to address the variations in strain rate and pressure that affect premixed flamelets, diffusion flamelets, and multi-branched flamelets.

3. Computational results and discussion

The ordinary differential equations are solved numerically using a relaxation method with a pseudo-time variable and central differences. The parameters that are varied are K, Pr, ω_κ and S_1 (and thereby $S_2 = 1 - S_1$). Here, calculations have $Sc = Pr = 1$ with emphasis on the effect of variation in K, i.e. pressure and strain rate.

Here, the effects of vorticity on three types of oxygen-propane flame structure will be examined. In Subsection 3.1, a diffusion flame near its flammability is considered. The premixed flame is discussed in Subsection 3.2 while the multi-branched flame calculations are shown in Subsection 3.3. The basic calculations pertain to the inward swirling flow

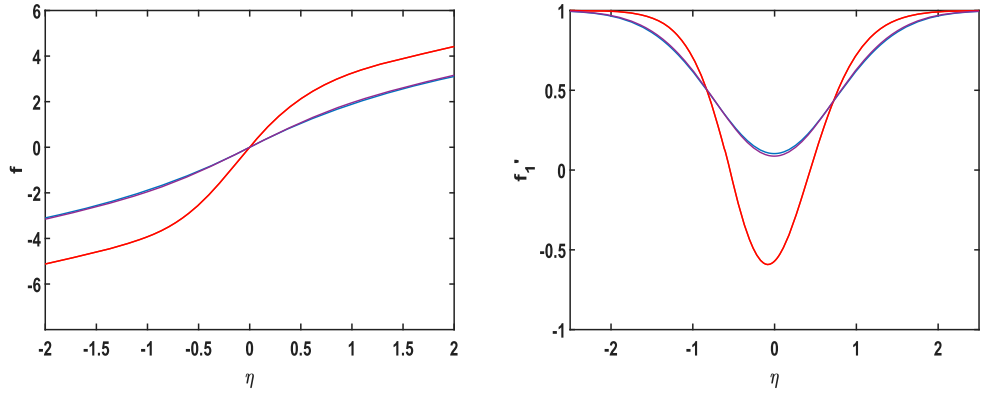

(a) mass flux per area, $f = \rho u_\chi$ (b) velocity component, $f_1' = u_\xi/(S_1\xi)$

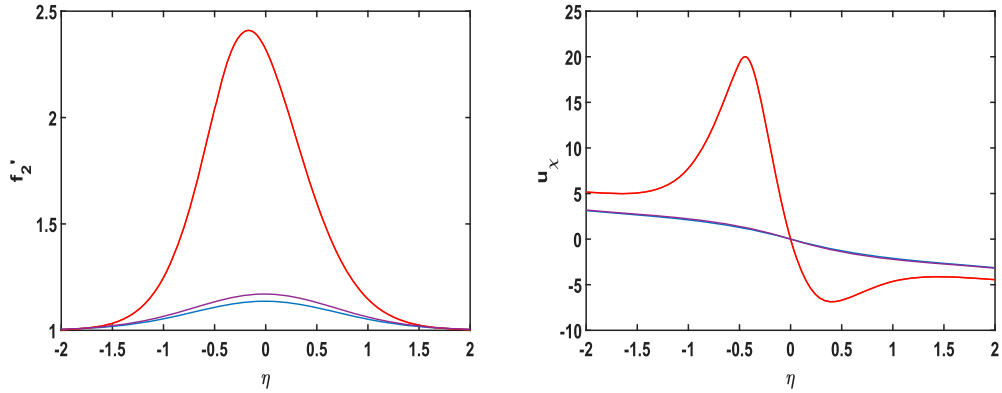

(c) velocity component, $f_2' = w/(S_2 z)$ (d) velocity component, u_χ

Figure 3. Velocity behaviour for diffusion flame with varying vorticity. $S_1 = -1.00$; $S_2 = 2.00$; $K = 0.275$. $\omega_\kappa = 0$, blue, no flame; $\omega_\kappa = 0.5$, purple, no flame; $\omega_\kappa = 1.0$, red, flame, flow reversal. (a) mass flux per area, $f = \rho u_\chi$; (b) velocity component, $f_1' = u_\xi/(S_1\xi)$; (c) velocity component, $f_2' = w/(S_2 z)$; (d) velocity component, u_χ.

with $Pr = Sc = 1$ and equal compressive strain rate in the far field from two directions in the rotating frame of reference, i.e. $S_1 = -1.0$ and $S_2 = 2.0$. Note that the same code for these calculations was used by [10] where both S_1 and S_2 were positive. Values for $K = Da/Da_{ref}$ and thereby for the Damköhler number Da are deliberately chosen in the vicinity of the flammability limit where vorticity and its centrifugal effect can be significant. In addition to boundary values at $\eta = \infty$ and $\eta = -\infty$, the system of equations has four independent, non-dimensional parameters as inputs: $\omega_\kappa, S_1 = 1 - S_2, Pr = Sc$, and $Da = KDa_{ref}$.

3.1. *Diffusion flamelet calculations*

First, we treat a situation with a three-dimensional diffusion-flame structure. Figures 2 and 3 show the influence of vorticity on the flamelet stability near the extinction limit. The rotation of the flamelet due to vorticity causes a centrifugal effect on the counterflow velocity and thereby on the residence time in the vicinity of the reaction zone. $K = 0.275$ with values of $\omega_\kappa = 0, 0.5$, and 1.0 are examined and reported here.

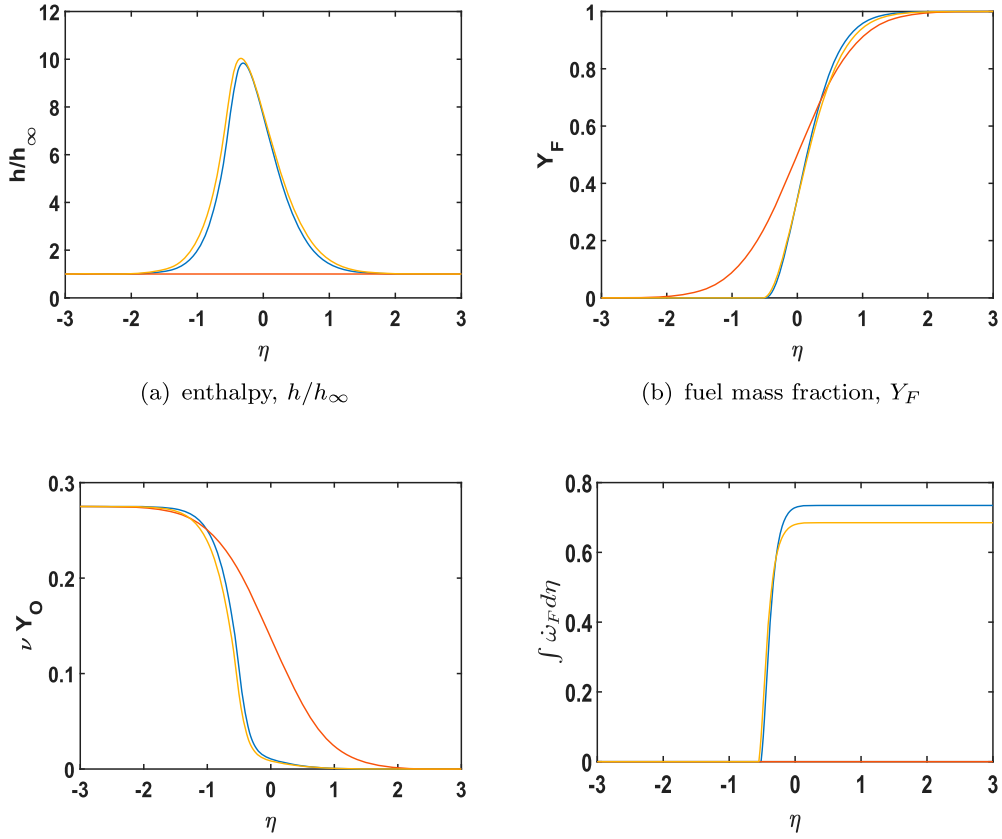

(a) enthalpy, h/h_∞ (b) fuel mass fraction, Y_F

(c) mass ratio x oxygen mass fraction, νY_O (d) integral of reaction rate, $\int \dot{\omega}_F d\eta$

Figure 4. Effects of normal strain on scalar properties for diffusion flame. $K = 0.275$; $\omega_\kappa = 1.0$. $S_1 = -1.25$, $S_2 = 2.25$: red, no flame. $S_1 = -1.00$, $S_2 = 2.00$: blue, flame. $S_1 = -0.75$, $S_2 = 1.75$: orange, flame. (a) enthalpy, h/h_∞; (b) fuel mass fraction, Y_F; (c) mass ratio x oxygen mass fraction, νY_O; (d) integral of reaction rate, $\int \dot{\omega}_F \mathrm{d}\eta$.

Figure 2 shows that, without rotation and also with $\omega_\kappa = 0.5$, there is negligible reaction rate and heat release, essentially yielding extinction. Fuel and oxidiser just diffuse and mix without significant exothermic reaction. Further increase of the rotational rate with $\omega_\kappa = 1.0$, however, yields a strong flame with a narrow reaction zone.

The heat release causes a decrease of the density in the vicinity of the flame. A plane still exists in the rotating reference frame where two different mixtures come together in a direction aligned with the scalar gradient while turning into the z direction aligned with the vorticity. The expanding gas can cause a flow reversal of the inward flow from the ξ-direction, orthogonal to the scalar gradient, as shown in Figure 3. The increased rotational rate produces the centrifugal acceleration that inhibits radially inward flow of the heavier gas and allows the expansion and velocity reversal for the lighter, hotter gas. Note that the development of negative values for f_1' means that with the value $S_1 \leq 0$, the direction of the velocity component u_ξ becomes radially outward, i.e. $u_\xi > 0$ for $\xi > 0$ and $u_\xi < 0$ for $\xi < 0$.

Clearly, the combination of fluid rotation, variable density, and three-dimensional structure have major consequences for flamelet behaviour. The specific mechanism is not immediately obvious but can be inferred from the results. Figure 3(b,c) indicate that the strong swirl causes the reversal of the u_ξ velocity and an increase in the w velocity, both

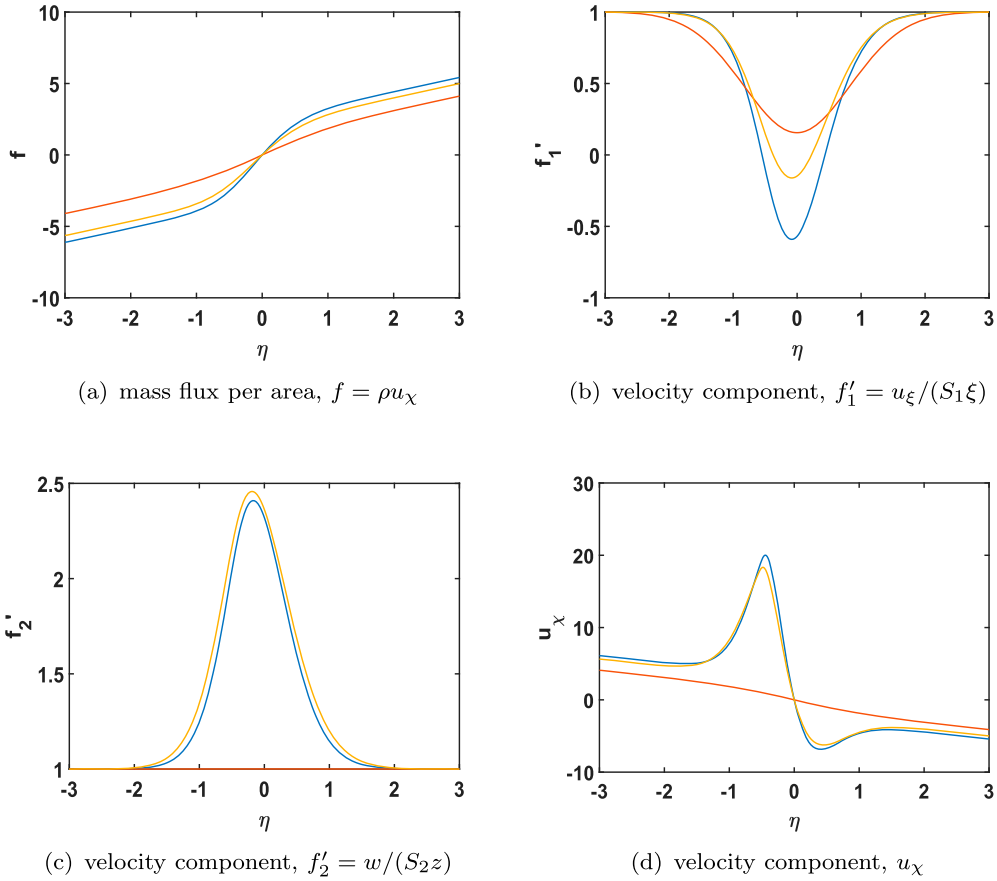

(a) mass flux per area, $f = \rho u_\chi$

(b) velocity component, $f_1' = u_\xi/(S_1\xi)$

(c) velocity component, $f_2' = w/(S_2 z)$

(d) velocity component, u_χ

Figure 5. Effects of normal strain on flow properties for diffusion flame. $K = 0.275$; $\omega_\kappa = 1.0$. $S_1 = -1.25$, $S_2 = 2.25$: red, no flame. $S_1 = -1.00$, $S_2 = 2.00$: blue, flame, flow reversal. $S_1 = -0.75$, $S_2 = 1.75$: orange, flame, flow reversal. (a) mass flux per area, $f = \rho u_\chi$; (b) velocity component, $f_1' = u_\xi/(S_1\xi)$; (c) velocity component, $f_2' = w/(S_2 z)$; (d) velocity component, u_χ.

now being outward flows from the combustion zone. However, the fractional decrease in density implied by Figure 2(a) is significantly larger than the fractional increase in outward velocity. So, the outward mass flow rate is reduced which is consistent with the reduction of the inward mass flow rate when the inward flow ceases to come from both the ξ and χ directions and is limited to only the χ direction. Thereby, an increase in residence time of the flow in the reaction domain is allowed. This increase in vorticity and thereby in swirl rate changes the flammability limit.

In Figures 4 and 5, the effect of the imposed ambient normal strain rates is examined for a situation with $\omega_\kappa = 1$. Flame extinction results in this example with an increase of the magnitude of the ξ normal strain rate S_1 beyond the value of the χ normal strain rate. So, $S_1 + S_2 = 1 < |S_1| = 1.25$ yields no flame while a strong flame is established for the two cases where $S_1 + S_2 = 1 \geq |S_1|$. Modest decreases in the integrated reaction rate, the mass flux f, and the amount of flow reversal occur with a reduction of imposed strain in the ξ direction from the base case where $S_1 = -1.0$; simultaneously, a modest increase in peak temperature and enthalpy occurs. Apparently, the reduced mass flux and associated increase in residence time allows for a slightly greater temperature rise although the reaction rate is slightly reduced. On the other hand, the increase in the magnitude of S_1 from the base case would, if density were reduced because of an established flame, yield too low a residence time to hold a flame; so, no flame occurs.

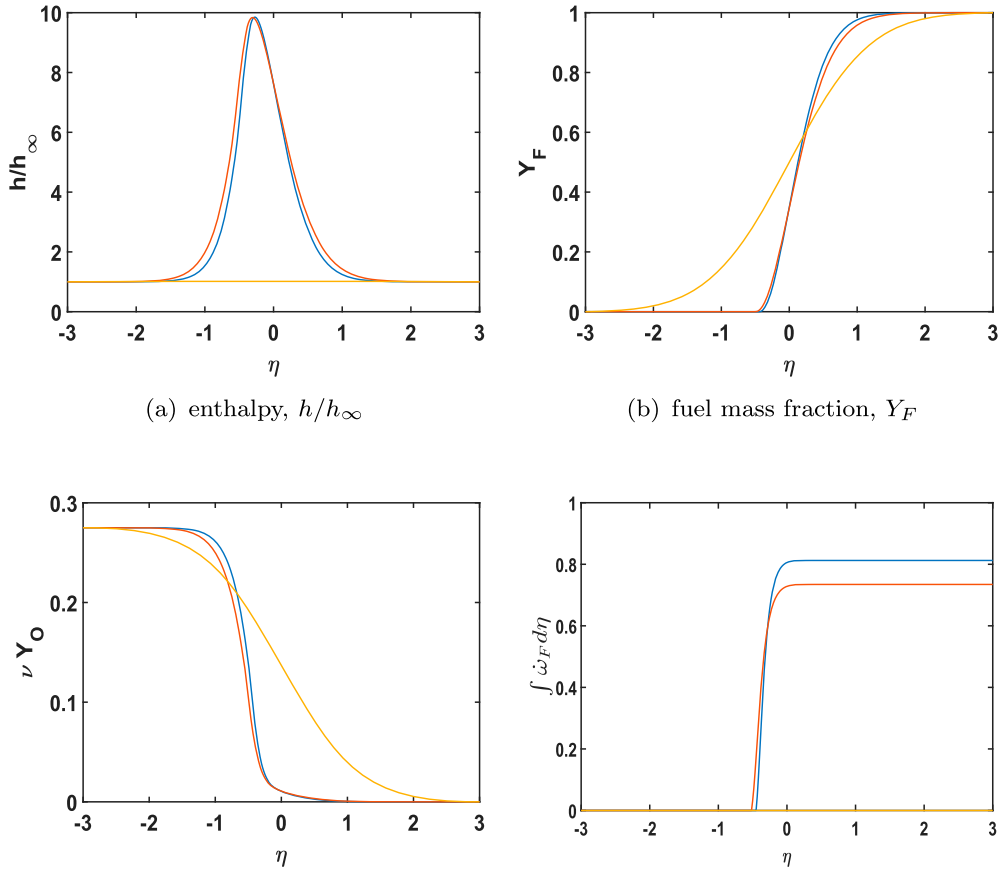

(a) enthalpy, h/h_∞ (b) fuel mass fraction, Y_F

(c) mass ratio x oxygen mass fraction, νY_O (d) integral of reaction rate, $\int \dot{\omega}_F d\eta$

Figure 6. Effects of Prandtl number on scalar properties for diffusion flame. $K = 0.275$; $\omega_\kappa = 1.0$; $S_1 = -1.00$; $S_2 = 2.00$. $Pr = 1.3$: blue, flame. $Pr = 1.0$: red, flame. $Pr = 0.7$: orange, no flame. (a) enthalpy, h/h_∞; (b) fuel mass fraction, Y_F; (c) mass ratio x oxygen mass fraction, νY_O; (d) integral of reaction rate, $\int \dot{\omega}_F \mathrm{d}\eta$.

The sensitivity to thermal and mass diffusivities is shown in Figures 6 and 7. These diffusivities increase as the Prandtl number Pr decreases. Thus, higher Pr results in thinner diffusion layers as shown in the figures. However, when the diffusivity is too large, heat is carried away over too large a domain to maintain a flame.

The comparison of the results here for diffusion flames with the results of the earlier rotational flamelet model without inward swirl [10] are interesting. Here, an approximately 40-per-cent-larger value of Da is needed to prevent extinction. The incoming flow from two directions apparently has a shorter residence time for the same strain rate. The qualitative nature of the results as functions of η are similar for the two models. However, the directions of the three-dimensional velocity components relate to critical physics and are consequential.

3.2. *Premixed flamelet calculations*

The analysis can apply to a situation where the inward swirling fluid has opposing streams of a combustible mixture and a hot inert gas (likely combustion products). A premixed flame can be established. As noted in an early study for counterflow flamelet [10], the

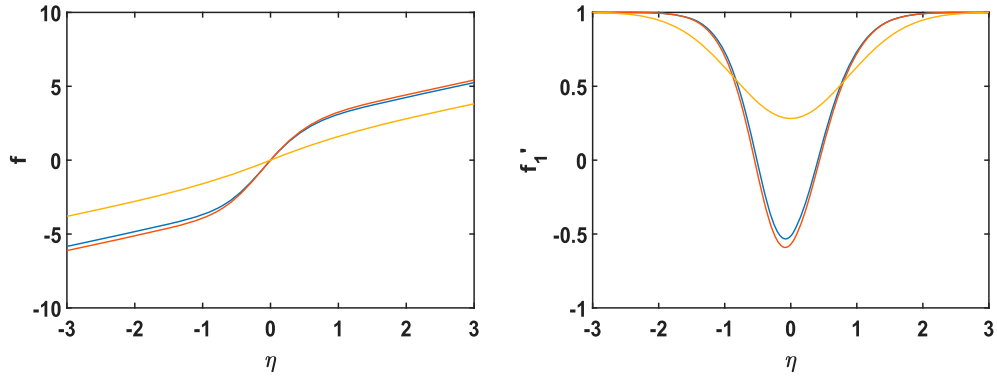

(a) mass flux per area, $f = \rho u_\chi$ (b) velocity component, $f_1' = u_\xi/(S_1\xi)$

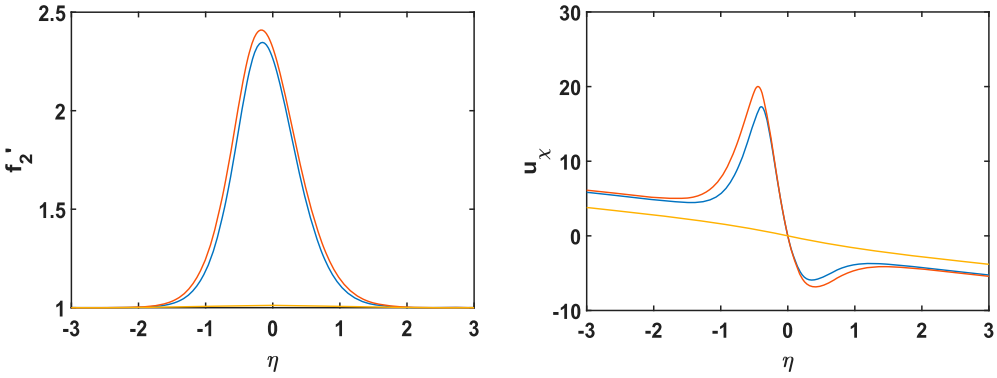

(c) velocity component, $f_2' = w/(S_2 z)$ (d) velocity component, u_χ

Figure 7. Effects of Prandtl number on flow properties for diffusion flame. $K = 0.275$; $\omega_\kappa = 1.0$; $S_1 = -1.00$; $S_2 = 2.00$. $Pr = 1.3$: blue, flame, flow reversal. $Pr = 1.0$: red, flame, flow reversal. $Pr = 0.7$: orange, no flame, no flow reversal. (a) mass flux per area, $f = \rho u_\chi$; (b) velocity component, $f_1' = u_\xi/(S_1\xi)$; (c) velocity component, $f_2' = w/(S_2 z)$; (d) velocity component, u_χ.

premixed flame requires a *Da* value that is orders of magnitude larger than the required value for a diffusion flame. The vorticity and centrifugal motion can have consequence, especially near a flammability limit. Figures 8 and 9 have some interesting results. At a *Da* value of one-hundred to two-hundred-fifty times the reference value, i.e. $K = 100$, 200, 250, a strong premixed flame is shown to exist with or without a vorticity field. Application of swirl through the vorticity results in the same peak enthalpy or temperature and nearly the same flame speed (in the χ direction). The ξ component of velocity is seen to reverse direction with or without imposed vorticity. However, the increase in rotational rate and centrifugal acceleration decreases the magnitude of the reversal. The premixed flame moves slightly farther upstream as measured by the η value as swirl is applied. It likely occurs because, with less reversal in the ξ direction, the expansion in the η direction is enhanced.

A decrease in *Da* to a situation where $K = 20$ results in extinction with vorticity in the range up to $\omega_\kappa = 1.0$. That situation is studied further with examination of the effect of vorticity on the extinction of the flame. Results in Figures 10 and 11 show four cases with $K = 37.5$ and ω_κ varying between 0 and 1.5. For $0.5 \geq \omega_\kappa \geq 0$, a flame cannot survive

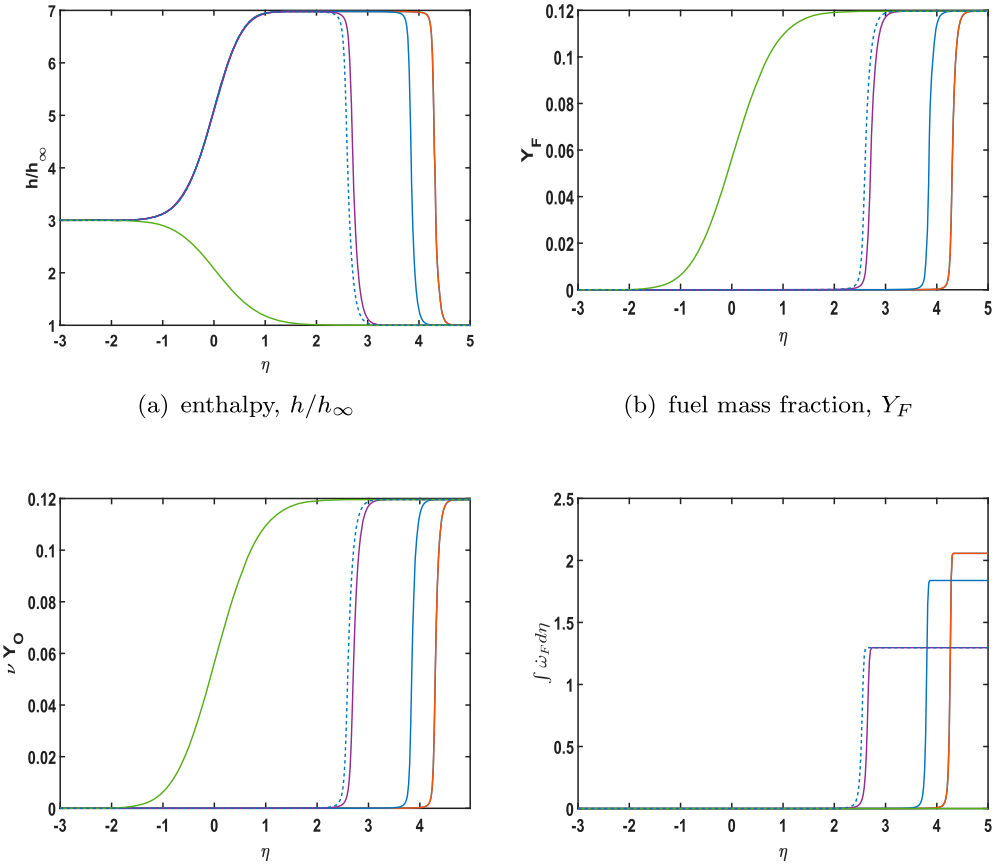

(a) enthalpy, h/h_∞ (b) fuel mass fraction, Y_F

(c) mass ratio x oxygen mass fraction, νY_O (d) integral of reaction rate, $\int \dot{\omega}_F d\eta$

Figure 8. Scalar properties for premixed flame with varying Damköhler number and vorticity. $S_1 = -1.00$, $S_2 = 2.00$. $K = 250$, $\omega_\kappa = 1.0$, red, flame; $K = 200$, $\omega_\kappa = 1.0$, blue, flame; $K = 100$, $\omega_\kappa = 1.0$, purple, flame; $K = 100$, $\omega_\kappa = 0$, dash blue, flame; $K = 20, \omega_\kappa = 1.0$, green, no flame. (a) enthalpy, h/h_∞; (b) fuel mass fraction, Y_F; (c) mass ratio x oxygen mass fraction, νY_O; (d) integral of reaction rate, $\int \dot{\omega}_F \mathrm{d}\eta$.

while, for $\omega_\kappa \geq 1.0$, a strong premixed flame exists. In the range where a flame exists, the burning rate flame speed increases slightly as the vorticity magnitude increases. Due to the centrifugal effect, u_ξ decreases in the flame region as ω_κ increases. In fact, it reverses direction near the flame. However, u_χ increases with ω_κ so the mass flux and burning rate increase as well.

It is seen here for the premixed flame, as well as for the diffusion flame, that the rotational flamelet with inward flow in one direction only [10] can avoid extinction at lower values of *Da* than is possible for the inward swirling flamelet.

3.3. *Multi-branched flamelet calculations*

Recent works have addressed the structure of multi-branched flamelets with a central diffusion flame and one or two premixed flames. The premixed flames can be fuel rich or fuel lean. They might be driven by heat transfer from the stronger diffusion flame. With three flames, the diffusion flame is centred between the two premixed flames and has the highest temperature. See [10,26,29] which address three general configurations: a stagnation flow, counterflow imposed on a shear layer,and a rotational flamelet. Here, we examine the

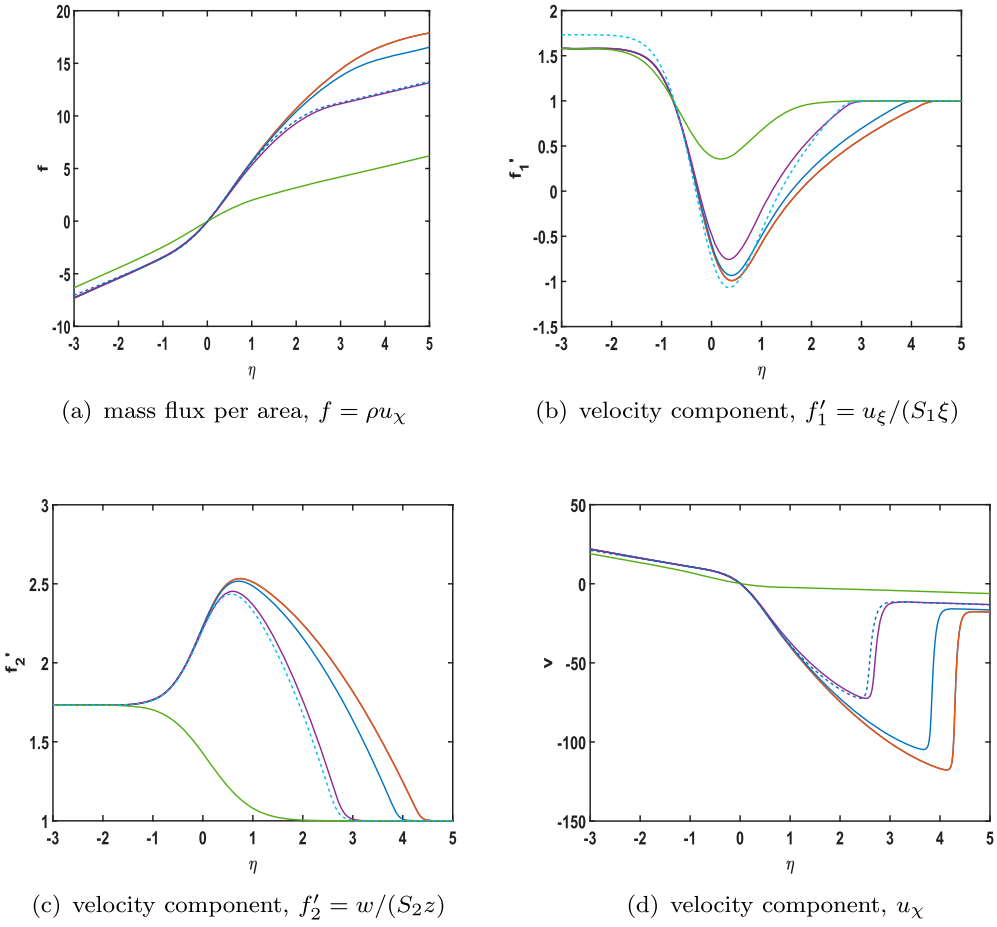

(a) mass flux per area, $f = \rho u_\chi$

(b) velocity component, $f_1' = u_\xi/(S_1\xi)$

(c) velocity component, $f_2' = w/(S_2 z)$

(d) velocity component, u_χ

Figure 9. Velocity behaviour for premixed flame with varying Damköhler number and vorticity. $S_1 = -1.00$, $S_2 = 2.00$. $K = 250$, $\omega_\kappa = 1.0$, red, flame; $K = 200$, $\omega_\kappa = 1.0$, blue, flame; $K = 100$, $\omega_\kappa = 1.0$, purple, flame; $K = 100$, $\omega_\kappa = 0$, dash blue, flame; $K = 20, \omega_\kappa = 1.0$, green, no flame. (a) mass flux per area, $f = \rho u_\chi$; (b) velocity component, $f_1' = u_\xi/(S_1\xi)$; (c) velocity component, $f_2' = w/(S_2 z)$; (d) velocity component, u_χ.

multi-flame structure and behaviour for the inward-swirling flamelet. Figures 12 and 13 show the computational results for relatively high values of *Da*. Later, Figures 14 and 15 will address the structure and behaviour for values of *Da* near the flammability limits. The effects of vorticity are especially of interest.

It is sometimes convenient to present the flamelet scalar variables as functions of a conserved scalar instead of as a function of the spatial coordinate. For our simple, one-step kinetics calculations, conserved scalars are formed by defining the Shvab Zel'dovich variables $\alpha \equiv Y_F - \nu Y_O$ and $\beta \equiv h + \nu Y_O \tilde{Q}$ where $\tilde{Q}$ is the fuel heating value normalised by $h^*(\infty)$. Then, Equation (13) yields

$$\begin{aligned} \alpha'' + Pr(S_1 f_1 + S_2 f_2)\alpha' &= 0 \\ \beta'' + Pr(S_1 f_1 + S_2 f_2)\beta' &= 0 \end{aligned} \tag{19}$$

In the above relations, the required constants are $S_1, S_2 = 1 - S_1, \rho_{-\infty}, \nu, \tilde{Q}, Pr$. Solutions are coupled to the simultaneous solutions of Equation (11). A normalised conserved scalar

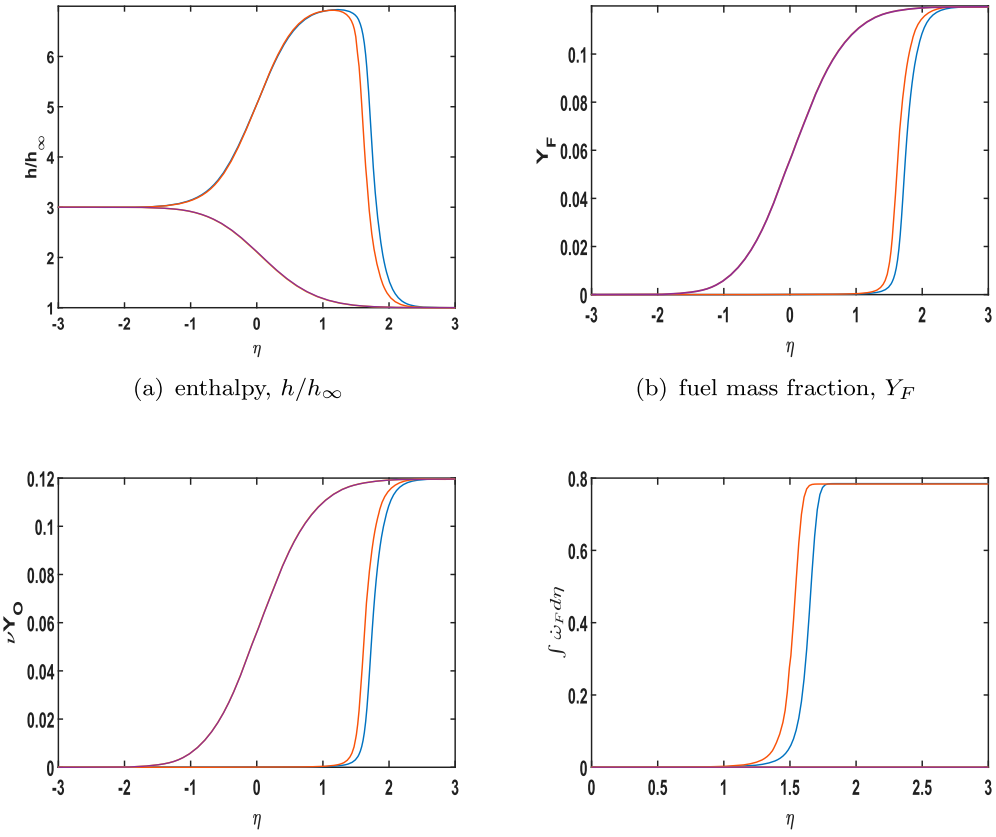

(a) enthalpy, h/h_∞ (b) fuel mass fraction, Y_F

(c) mass ratio x oxygen mass fraction, νY_O (d) integral of reaction rate, $\int \dot{\omega}_F d\eta$

Figure 10. Scalar properties for premixed flame for premixed flame with varying vorticity near extinction value for Damköhler number. $K = 37.5$, $S_1 = -1.00$, $S_2 = 2.00$. $\omega_\kappa = 1.5$, blue, flame; $\omega_\kappa = 1.0$, red, flame; $\omega_\kappa = 0.5$, purple, no flame; $\omega_\kappa = 0$, dash blue (sometimes covered by purple), no flame. (a) enthalpy, h/h_∞; (b) fuel mass fraction, Y_F; (c) mass ratio x oxygen mass fraction, νY_O; (d) integral of reaction rate, $\int \dot{\omega}_F \mathrm{d}\eta$.

Σ varying between the values of 0 and 1 can be formed as shown by Sirignano.

$$\Sigma \equiv \frac{\alpha - \alpha_{-\infty}}{\alpha_\infty - \alpha_{-\infty}} = \frac{\beta - \beta_{-\infty}}{\beta_\infty - \beta_{-\infty}} \tag{20}$$

The use of plots of scalar variables as a function of Σ are helpful in identifying the location of reaction zones in the flame structure.

In Figures 14 and 15, results are shown for a configuration with a fuel-rich mixture at $\eta = \infty$ and a fuel-lean situation at $\eta = -\infty$. The fuel-rich mixture exists with $Y_F = 2/3$ and $Y_O = 1/3$ flows inward on one side of the swirling flame and a fuel-lean mixture with $Y_F = 1/12$ and $Y_O = 11/12$ flows inward from the other side.

For a sufficiently high value of Da, a strong diffusion flame and a weak, fuel-rich premixed can co-exist without a rotational flow. See the case with $K = 0.180$ and $\omega_\kappa = 0$ in the figures. The weak premixed flame is indicated by the region of negative second derivative for enthalpy on the right-side of Figure 14(e). (A negative second derivative also exists on the right-side of Figure 14(a) but is more difficult to detect.) In Figure 14(d), the diffusion flame contributes to the region with the largest first derivative (the reaction rate which is the integrand) while the premixed flame contributes in the region where the first

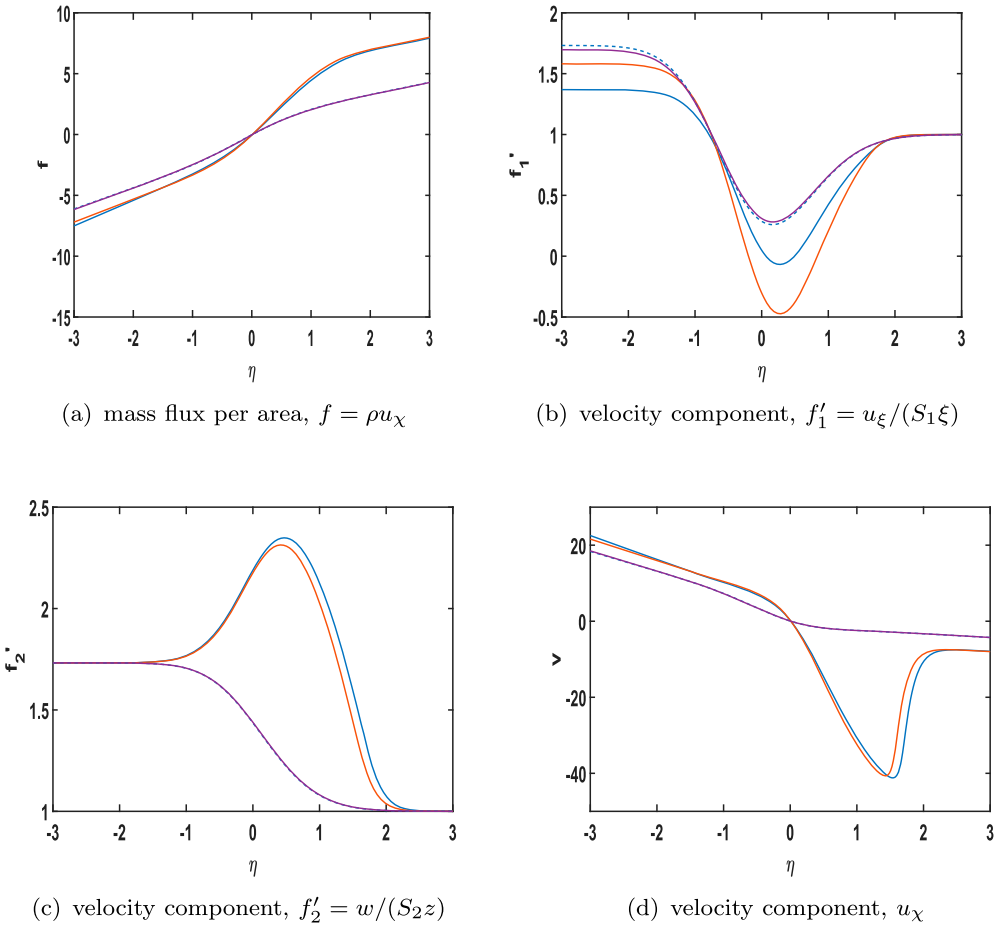

(a) mass flux per area, $f = \rho u_\chi$

(b) velocity component, $f_1' = u_\xi/(S_1\xi)$

(c) velocity component, $f_2' = w/(S_2 z)$

(d) velocity component, u_χ

Figure 11. Velocity behaviour for premixed flame with varying vorticity near extinction value for Damköhler number. $K = 37.5$, $S_1 = -1.00$, $S_2 = 2.00$. $\omega_\kappa = 1.5$, blue, flame; $\omega_\kappa = 1.0$, red, flame; $\omega_\kappa = 0.5$, purple, no flame; $\omega_\kappa = 0$, dash blue (sometimes covered by purple), no flame. (a) mass flux per area, $f = \rho u_\chi$; (b) velocity component, $f_1' = u_\xi/(S_1\xi)$; (c) velocity component, $f_2' = w/(S_2 z)$; (d) velocity component, u_χ.

derivative is still positive but smaller. The existence of multiple flames is also indicated by consumption of oxygen to the right of the diffusion flame in 14(c). The weak premixed flame is driven by heat diffusion from the strong diffusion flame. The heating from the diffusion flame allows the premixed flame to exist in the multi-branched structure at values of *Da* where a premixed flame could not survive independently in isolated fashion. More information about these multi-flame structures is provided by [29].

For the reduced values of Damköhler number *Da*, rotation is needed to produce a flame. For example, as the same figures show with $K = 0.170$, a strong flame appears with $\omega_\kappa = 0.75$ but there is no flame development possible with $\omega_\kappa \leq 0.5$. Similarly, for still smaller *Da*, even greater rotational rate is needed; for $K = 0.160, \omega_\kappa = 1.50$ produces a strong flame, while for $\omega_\kappa \leq 1.00$, no flame is sustained with any vorticity value.

Figure 15(b) indicates that a strong flame will cause flow reversal in the ξ direction due to gas expansion.

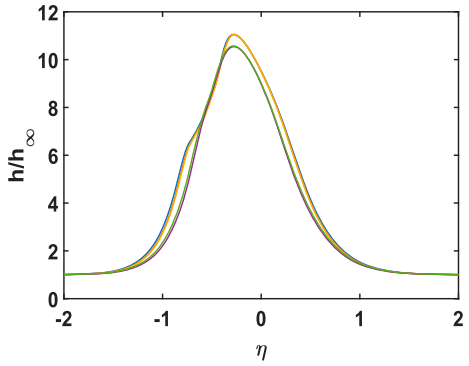

(a) enthalpy, h/h_∞

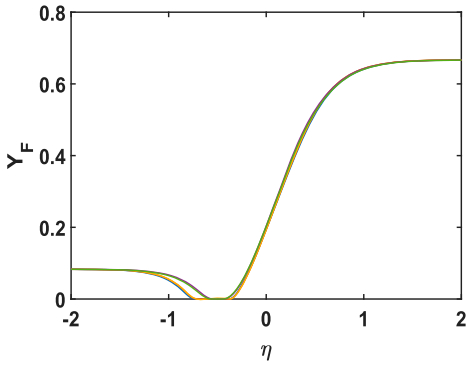

(b) fuel mass fraction, Y_F

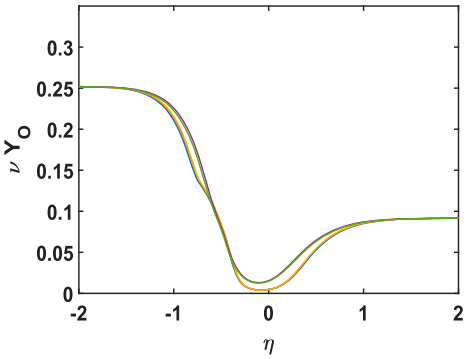

(c) mass ratio x oxygen mass fraction, νY_O

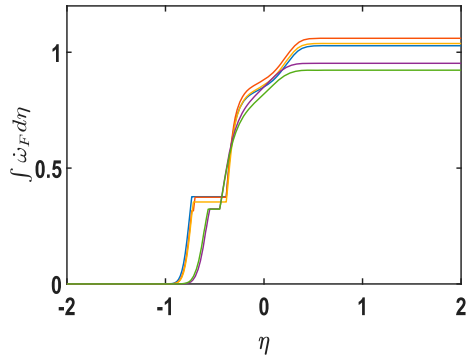

(d) integral of reaction rate, $\int \dot{\omega}_F d\eta$

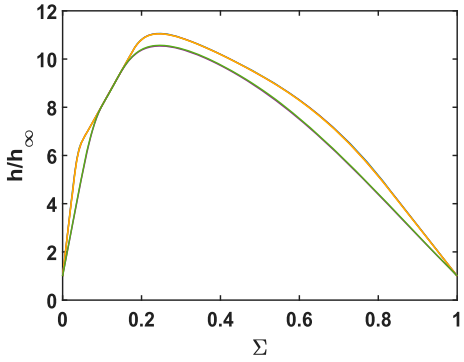

(e) enthalpy, h/h_∞, versus conserved scalar, Σ

Figure 12. Scalar properties for multibranched flame with varying Damköhler number and vorticity. $S_1 = -1.00, S_2 = 2.00$. $K = 1.00$: $\omega_\kappa = 1.0$, blue; $\omega_\kappa = 0.50$, red; $\omega_\kappa = 0$, orange. $K = 0.300$: $\omega_\kappa = 1.0$, green; $\omega_\kappa = 0$, purple. (a) enthalpy, h/h_∞; (b) fuel mass fraction, Y_F; (c) mass ratio x oxygen mass fraction, νY_O; (d) integral of reaction rate, $\int \dot{\omega}_F \mathrm{d}\eta$; (e) enthalpy, h/h_∞, versus conserved scalar, Σ.

4. Conclusions

A new flamelet model is developed to treat a range of flame structures in a steady, stretched, three-dimensional vortex. Non-premixed flames, premixed flames, and multi-branched flames are addressed through a unified theory. The creation of a contrived parameter such as a progress variable is avoided. Four nondimensional parameters are controlling: the

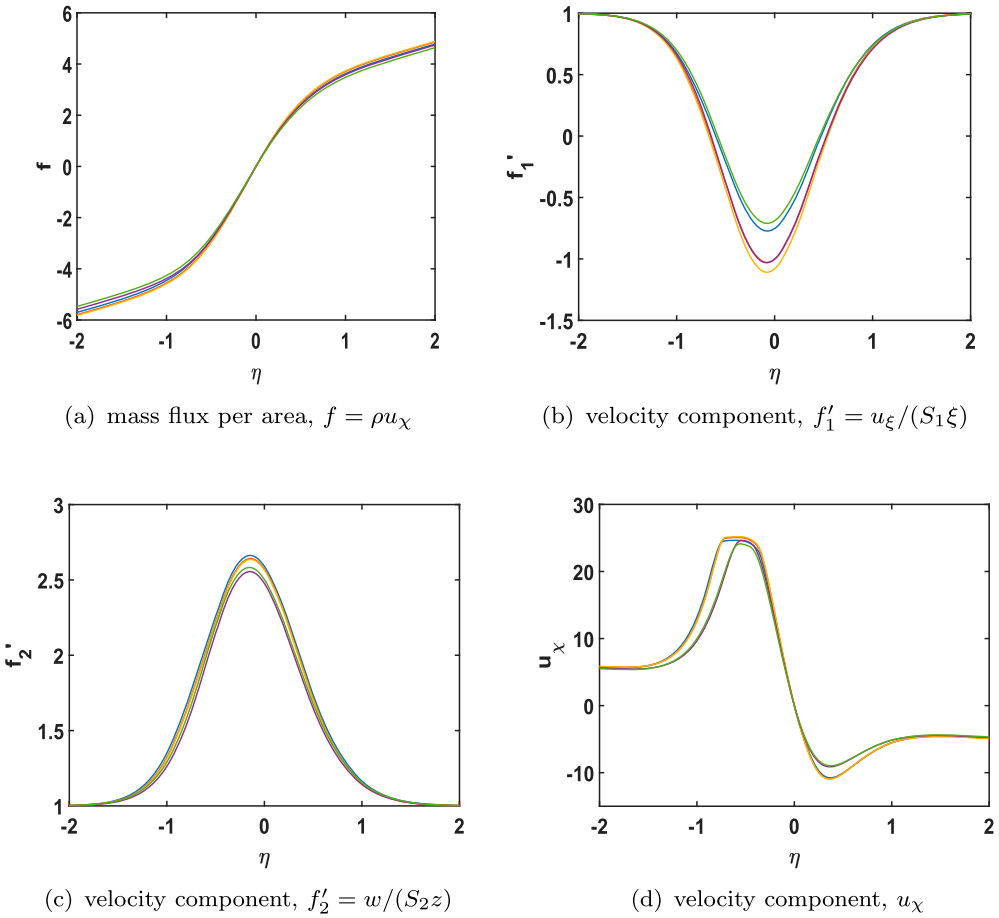

(a) mass flux per area, $f = \rho u_\chi$

(b) velocity component, $f_1' = u_\xi/(S_1\xi)$

(c) velocity component, $f_2' = w/(S_2 z)$

(d) velocity component, u_χ

Figure 13. Velocity behaviour for multibranched flame with varying Damköhler number and vorticity. $S_1 = -1.00, S_2 = 2.00$. $K = 1.00$: $\omega_\kappa = 1.0$, blue; $\omega_\kappa = 0.50$, red; $\omega_\kappa = 0$, orange. $K = 0.300$: $\omega_\kappa = 1.0$, green; $\omega_\kappa = 0$, purple. (a) mass flux per area, $f = \rho u_\chi$; (b) velocity component, $f_1' = u_\xi/(S_1\xi)$; (c) velocity component, $f_2' = w/(S_2 z)$; (d) velocity component, u_χ.

imposed, normalised compressive strain rate S_1; the imposed,normalised vorticity ω_κ; the Damköhler number *Da*; and the Prandtl number *Pr* which equals the Schmidt number *Sc* here. The effects of these quantities are shown in the computational results. While this new theory is established for multi-step oxidation chemistry, a simple example of one-step, propane-oxygen kinetics is considered.

The model is developed with an analysis that parallels the method for the rotational flamelet [10]; however, the essential physical difference is in the applied normal strain rates and the resulting flow directions for the three velocity components. Both models involve a stretched vortex. However, This new model has inflow in two directions and outflow in one direction whereas the prior work had only one inflow direction. This difference results in the inward swirling flow which modifies the important centrifugal effect that appears when vorticity, variable density, and three-dimensional structure are interactive. The early work of [4] was pioneering and did involve inward swirl modelled after Burgers work [19]. A three-dimensional structure and spatially varying density were not examined there; thus, the vital centrifugal motion was not included.

The effects of the inward swirl inherent to the stretched vortex are shown to be significant, especially in modifying the flammability limits. Variable density is shown to have a

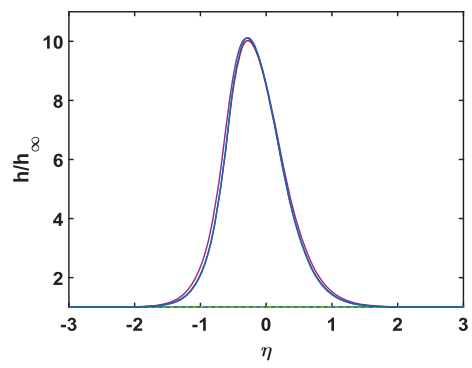

(a) enthalpy, h/h_∞

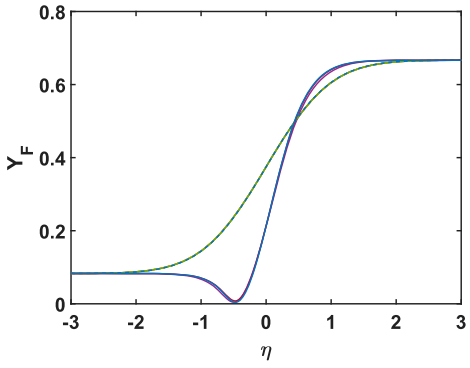

(b) fuel mass fraction, Y_F

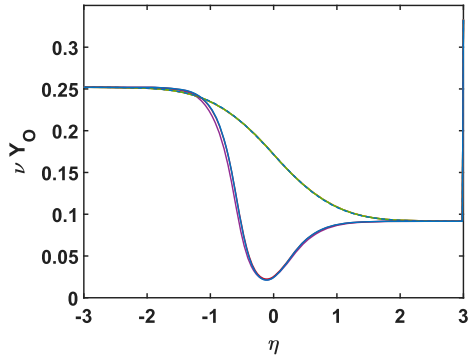

(c) mass ratio x oxygen mass fraction, νY_O

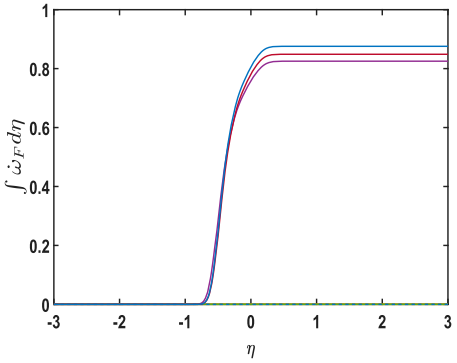

(d) integral of reaction rate, $\int \dot{\omega}_F d\eta$

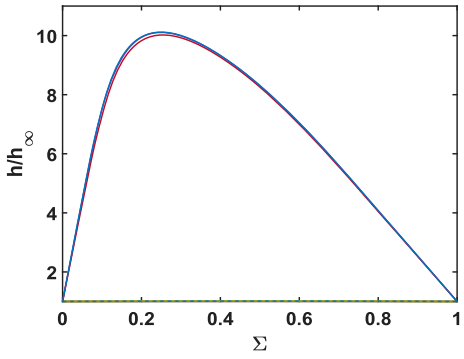

(e) enthalpy, h/h_∞, versus conserved scalar, Σ

Figure 14. Scalar properties for multibranched flame with varying vorticity. $S_1 = -1.00, S_2 = 2.00$. Cases with a strong flame: $K = 0.180, \omega_\kappa = 0$, solid blue; $K = 0.170, \omega_\kappa = 0.75$, red; $K = 0.160, \omega_\kappa = 1.50$, purple. Other curves show no flame (extinction) and all fall on the dashed blue line: $K = 0.170, \omega_\kappa = 0.50$; $K = 0.160, \omega_\kappa = 1.00$. (a) enthalpy, h/h_∞; (b) fuel mass fraction, Y_F; (c) mass ratio x oxygen mass fraction, νY_O; (d) integral of reaction rate, $\int \dot{\omega}_F \mathrm{d}\eta$; (e) enthalpy, h/h_∞, versus conserved scalar, Σ.

critical role since the centrifugal force created through the vorticity has impact in that case. In order to avoid extinction, premixed flames require a minimum value of Damköhler number *Da* (or, equivalently, maximum normal strain rate value) that is orders of magnitude

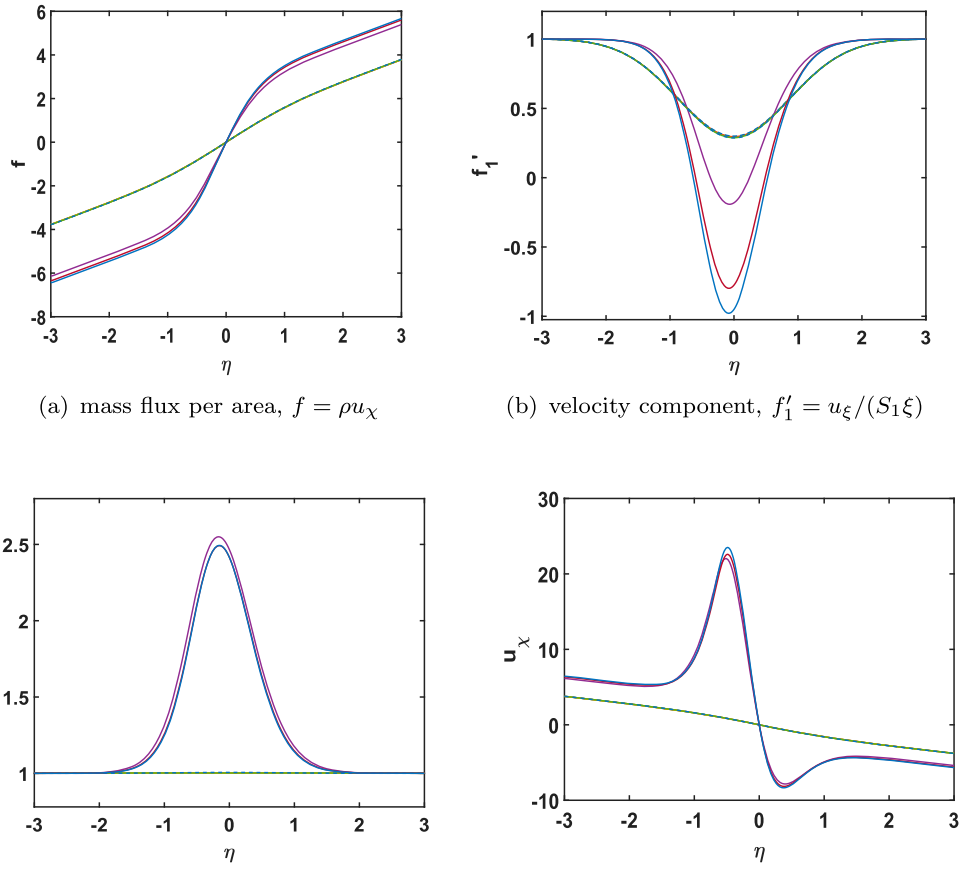

(a) mass flux per area, $f = \rho u_\chi$

(b) velocity component, $f_1' = u_\xi/(S_1\xi)$

(c) velocity component, $f_2' = w/(S_2 z)$

(d) velocity component, u_χ

Figure 15. Velocity behaviour with varying vorticity for multibranched flame. $S_1 = -1.00; S_2 = 2.00$. Cases with a strong flame: $K = 0.180, \omega_\kappa = 0$, solid blue; $K = 0.170, \omega_\kappa = 0.75$, red; $K = 0.160, \omega_\kappa = 1.50$, purple. Other curves show no flame (extinction) and all fall on the dashed blue line: $K = 0.170, \omega_\kappa = 0.50$; $K = 0.160, \omega_\kappa = 1.00$. (a) mass flux per area, $f = \rho u_\chi$; (b) velocity component, $f_1' = u_\xi/(S_1\xi)$; (c) velocity component, $f_2' = w/(S_2 z)$; (d) velocity component, u_χ.

larger (smaller) than needed for diffusion flames or multi-flame structures. This conclusion is consistent with other models of flamelet-vortex interactions, e.g. the counterflow model [10] and the vortex-layer (or vortex-sheet) model [30] model. Thereby, the existence of subgrid premixed flamelets is quite small, possibly negligible.

For any of the flame structures, the increased vorticity can move the flammability limit to lower *Da* values. Higher *Da* (for proper ambient mixtures) makes multi-branched flames more likely. Heat from the diffusion flame can drive the premixed flames. The distribution of the normal compressive strain between the directions for incoming swirling flow can affect the results. The variation of *Pr* within the expected range can have some effect on the flammability limit.

Computational results here with inward swirl, when compared to the results for the rotational flamelet without the inward swirl [10], indicate that notably larger *Da* values are required to avoid extinction. One would expect that flamelets in turbulent combustion would thereby be less likely to form in vortex tubes that in other vortical structures.

For future studies, several issues are important. The computations should be extended to cases with detailed chemical kinetics, detailed transport models, and improved equations of state. Coupling of the flamelet model should be made with a RANS or LES analysis for a practical, reacting, mixing, shear flow. Direct numerical simulations of reacting flows that give improved correlations of resolved-scale velocity gradients with the smallest-scale velocity gradients would be helpful.

Disclosure statement

The author reports no conflict of interest.

Funding

The effort was supported by AFOSR through Award FA9550-18-1-0392 managed by Dr. Mitat Birkan.

References

[1] Linan A., The asymptotic structure of counterflow diffusion flames for large activation energies, Acta Astronaut. 1 (1974), pp. 1007–1039.
[2] Williams F.A., *Recent advances in theoretical descriptions of turbulent diffusion flames*, in *Turbulent Mixing in Nonreactive and Reactive Flows*, S.N.B. Murthy ed., Springer, New York, 1975, pp. 189–208.
[3] Marble F.E., *Growth of a diffusion flame in the field of a vortex*, in *Recent Advances in the Aerospace Sciences*, Plenum Press, New York, 1985, pp. 395–413.
[4] Karagozian A.R. and Marble F.E., Study of a diffusion flame in a stretched vortex, Combust. Sci. Technol. 45 (1986), pp. 65–84.
[5] Cetegen B.M. and Sirignano W.A., *Study of molecular mixing and a finite rate chemical reaction in a mixing layer*, in *Proceedings of Twenty-Second Symposium (International) on Combustion*, Combustion Institute, Pittsburgh, 1988, pp. 489–494.
[6] Cetegen B.M. and Sirignano W.A., Study of mixing and reaction in the field of a vortex, Combust. Sci. Technol. 72 (1990), pp. 157–181.
[7] Peters N., *Turbulent combustion*, 1st ed., Cambridge University Press, Cambridge, UK, 2000.
[8] Pierce C. and Moin P., Progress-variable approach for large-eddy simulation of non-premixed turbulent combustion, J. Fluid. Mech. 504 (2004), pp. 73–97.
[9] Williams F.A., Progress in knowledge of flamelet structure and extinction, Prog. Energy Combust. Sci. 26 (2000), pp. 657–682.
[10] Sirignano W.A., *Three-dimensional, rotational flamelet closure model with two-way coupling*, J. Fluid Mech. (2022). https://www.doi.org/10.1017/jfm.2022.562.
[11] Meneveau C. and Poinsot T., Stretching and quenching of flamelets in premixed turbulent combustion, Combust. Flame 86 (1991), pp. 311–332.
[12] Ihme M., Schmitt C., and Pitsch H., Optimal artificial neural networks and tabulation methods for chemistry representation in LES of a bluff-body swirl-stabilized flame, Proc. Combust. Inst. 32 (2009), pp. 1527–1535.
[13] Nguyen T., Popov P., and Sirignano W.A., Longitudinal combustion instability in a rocket motor with a single coaxial injector, J. Propuls. Power 34(2) (2018), pp. 354–373.
[14] Nguyen T. and Sirignano W.A., The impacts of three flamelet burning regimes in nonlinear combustion dynamics, invited paper, Combust. Flame 195 (2018), pp. 170–182.
[15] Nguyen T. and Sirignano W.A., Spontaneous and triggered longitudinal combustion instability in a rocket engine, AIAA J. 57 (2019), pp. 5351–5364.
[16] Shadram Z., Nguyen T.M., Sideris A., and Sirignano W.A., Neural network flame closure for a turbulent combustor with unsteady pressure, AIAA J. 59 (2021), pp. 621–635.
[17] Shadram Z., Nguyen T.M., Sideris A., and Sirignano W.A., Physics-aware neural network flame closure for combustion instability modeling in a single-Injector engine, Combust. Flame 240 (2022). pp.111973.

[18] Mueller M.E., Physically-derived reduced-order manifold-based modeling for multi-modal turbulent combustion, Combust. Flame 214 (2020), pp. 287–305.
[19] Burgers J.M., A mathematical model illustrating the theory of turbulence, Adv. Appl. Mech. 1 (1948), pp. 171–199.
[20] Rott N., On the viscous core of a line vortex, Z. Angew. Math. Phys. IXb (1958), pp. 543–553.
[21] Ashurst W.T., Kerstein A.R., Kerr R.M., and Gibson C.H., Alignment of vorticity and scalar gradient with strain rate in simulated Navier–Stokes turbulence, Phys. Fluids 30 (1987), pp. 2343–2352.
[22] Nomura K.K. and Elghobashi S.E., Mixing characteristics of an inhomogeneous scalar in isotropic and homogeneous sheared turbulence, Phys. Fluids A 4 (1992), pp. 606–625.
[23] Nomura K.K. and Elghobashi S.E., The structure of inhomogeneous turbulence scalar in variable density nonpremixed flames, Theor. Comput. Fluid Dyn. 5 (1993), pp. 153–175.
[24] Boratav O.N., Elghobashi S.E., and Zhong R., On the alignment of the a-strain and vorticity in turbulent nonpremixed flames, Phys. Fluids 8 (1996), pp. 2251–2253.
[25] Boratav O.N., Elghobashi S.E., and Zhong R., On the alignment of strain, vorticity and scalar gradient in turbulent, buoyant, nonpremixed flames, Phys. Fluids 10 (1998), pp. 2260–2267.
[26] Sirignano W.A., Mixing and combustion in a laminar shear layer with imposed counterflow, J. Fluid Mech. 908 (2021), pp. 1–33A35.
[27] Illingworth C.R., Steady flow in the laminar boundary layer of a gas, Proc. R. Soc. Lond. Ser. A 199 (1949), pp. 533–558.
[28] Westbrook C.K. and Dryer F.L., Chemical kinetic modeling of hydrocarbon combustion, Prog. Energy Combust. Sci.10 (1984), pp. 1–57.
[29] Sirignano W.A., *Diffusion-controlled premixed flames*, Combust. Theory Model., 25 (2021). Invited paper for special issue in honor of Professor Moshe Matalon.
[30] Sirignano W.A., *Stretched vortex layer flamelet*, Combust. Flame (2022). https://www.sciencedirect.com/science/article/abs/pii/S0010218022002917.